AECL EACL

AECL-11351, COG-95-296

# XPS, XRD and SEM Study of Oxidation of $UO_2$ by Air in Gamma Radiation at 150°C

# Analyses diffractométriques, par spectroscopie XPS, et par MEB de l'oxydation de l'$UO_2$ par l'air dans un champ de rayonnement gamma à 150°C

S. Sunder, N.H. Miller



June 1995 juin

# XPS, XRD AND SEM STUDY OF OXIDATION OF $UO_2$ BY AIR IN GAMMA RADIATION AT 150°C

by

S. Sunder and N.H. Miller

AECL
Whiteshell Laboratories
Pinawa, Manitoba, Canada R0E 1L0
1995

AECL-11351
COG-95-296

# XPS, XRD AND SEM STUDY OF OXIDATION OF $UO_2$ BY AIR IN GAMMA RADIATION AT 150°C

by

S. Sunder and N.H. Miller


## ABSTRACT

$UO_2$ disks were heated at 150°C in air, in $O_2$ with 60% saturated steam, and in Ar with 60% saturated steam atmospheres for ~2 years in gamma fields equivalent to those associated with 10- to 20-year-old used CANDU fuel. Surface analysis of the disks, using X-ray photoelectron spectroscopy, X-ray diffraction and scanning electron microscopy, shows formation of $U_3O_8$ on the $UO_2$ disks exposed to air or $O_2$. This is the first report of the formation of $U_3O_8$ on $UO_2$ by air oxidation at such a low temperature. The rate of $U_3O_8$ formation by dry air oxidation of $UO_2$ at 150°C and in gamma fields of dose rate ~15 $Gy \cdot h^{-1}$ is very low. The presence of water vapour along with $O_2$ increases the oxidation of $UO_2$ in gamma fields, leading to the formation of $U^{6+}$ phases, e.g., $UO_3 \cdot xH_2O$ along with $U_3O_8$. On the other hand, $UO_2$ disks did not suffer any oxidation by water vapour radiolysis at 150°C in an $O_2$-free (60% saturated steam in Ar) atmosphere. These are important observations for the dry storage of used fuel because the oxidation of $UO_2$ to $U_3O_8$ is accompanied by a volume expansion, which could result in splitting of the Zircaloy cladding and powdering of the fuel matrix.


AECL
Whiteshell Laboratories
Pinawa, Manitoba R0E 1L0
1995

AECL-11351
COG-95-296

# ANALYSES DIFFRACTOMÉTRIQUES, PAR SPECTROSCOPIE XPS, ET PAR MEB DE L'OXYDATION DE L'$UO_2$ PAR L'AIR DANS UN CHAMP DE RAYONNEMENT GAMMA À 150 °C

par

S. Sunder et N.H. Miller

## RÉSUMÉ

Des disques d'$UO_2$ ont été chauffés à 150 °C dans l'air et dans l'$UO_2$ en présence de vapeur saturée à 60 %, et dans l'Ar en atmosphères de vapeur saturée à 60 % pendant environ 2 années dans des champs de rayonnement gamma équivalents à ceux produits par du combustible CANDU irradié et stocké depuis 10 à 20 ans. L'analyse de la surface des disques, par les méthodes de spectroscopie de photoélectrons XPS, de diffraction des rayons X et de microscopie électronique à balayage a révélé la formation d'$U_3O_8$ sur les disques d'$UO_2$ mis en contact avec l'air ou l'$O_2$. Il s'agit de la première fois que l'on signale la formation d'$U_3O_8$ sur l'$UO_2$ par oxydation par l'air à une température aussi basse. La vitesse de formation d'$U_3O_8$ résultant de l'oxydation de l'$UO_2$ par l'air sec à 150 °C et dans des champs de rayonnement gamma à un débit d'environ 15 $Gy \cdot h^{-1}$ est très faible. La présence de vapeurs d'eau et d'$O_2$ accroît l'oxydation de l'$UO_2$ dans les champs de rayonnement gamma et conduit à la formation de phases $U^{6+}$, p. ex., $UO_3 \bullet x\ H_2O$ et $U_3O_8$. Par ailleurs, les disques d'$UO_2$ n'ont subi aucune oxydation par radiolyse de la vapeur d'eau à 150 °C en atmosphère exempte d'$O_2$ (vapeur saturée à 60 % dans l'Ar). Les faits observés revêtent une grande importance pour le stockage à sec du combustible irradié, car l'oxydation de l'$UO_2$ en $U_3O_8$ s'accompagne d'une dilatation qui pourrait conduire à l'éclatement de la gaine en Zircaloy et à la pulvérisation de la matrice de combustible.

EACL
Laboratoires de Whiteshell
Pinawa (Manitoba) R0E 1L0
1995

AECL-11351
COG-95-296

CONTENTS


| | | Page |
|---|---|---|
| 1. | INTRODUCTION | 1 |
| 2. | EXPERIMENTAL | 1 |
| | 2.1 MATERIALS | 1 |
| | 2.2 X-RAY PHOTOELECTRON SPECTROSCOPY | 6 |
| | 2.3 X-RAY DIFFRACTION | 6 |
| | 2.4 SCANNING ELECTRON MICROSCOPY | 6 |
| 3. | RESULTS AND DISCUSSION | 6 |
| | 3.1 VISUAL OBSERVATIONS | 6 |
| | 3.2 X-RAY PHOTOELECTRON SPECTROSCOPY | 7 |
| | 3.3 X-RAY DIFFRACTION | 13 |
| | 3.4 SCANNING ELECTRON MICROSCOPY | 20 |
| | 3.5 DISCUSSION | 20 |
| 4. | SUMMARY AND CONCLUSIONS | 27 |
| ACKNOWLEDGEMENTS | | 27 |
| REFERENCES | | 28 |
| APPENDIX A | | 33 |
| APPENDIX B | | 39 |

## LIST OF TABLES


| | | Page |
|---|---|---|
| 1. | XPS Results for the Surface Oxidation of $UO_2$ Disks at 150°C in Gamma Fields | 7 |
| 2. | Comparison of XPS and XRD Analysis of the Surface Oxidation of $UO_2$ Disks at 150°C in Gamma Fields | 19 |
| 3. | Calculation of Fraction of $U_3O_8$ Formation from XRD | 24 |
| B-1. | XRD Data for $UO_2$ Oxidation at 150°C in Gamma Radiation in Open Air (Sample M, Experiment A) | 41 |
| B-2. | XRD Data for $UO_2$ Oxidation at 150°C in Gamma Radiation in Closed Air (Sample L, Experiment B) | 43 |
| B-3. | XRD Data for $UO_2$ Oxidation at 150°C in Gamma Radiation ($O_2$ + 60% Saturated Steam; Sample X, Experiment C) | 45 |
| B-4. | XRD Data for $UO_2$ Oxidation at 150°C in Gamma Radiation (Ar + 60% Saturated Steam; Sample V, Experiment D) | 48 |

## LIST OF FIGURES


| | | Page |
|---|---|---|
| 1. | Schematic Diagrams of Glass Vials Used to Study Oxidation of $UO_2$ in Gamma Fields at High Temperatures: (a) Open to Atmosphere (Experiment A); (b) Sealed with Air (Experiment B); (c) Sealed with $O_2$ or Ar and Water (Experiments C and D) | 3 |
| 2. | Schematic Diagram of Experimental Set-up (Vessel with $UO_2$ Vials) | 4 |
| 3. | Schematic Diagram of the Relative Placement of the Vessels Containing $UO_2$ Samples and Used CANDU Fuel: A, Used Fuel Container; B, $UO_2$ Container; and C, IFTF Canister | 5 |
| 4. | XPS Spectra for the U 4f Region of $UO_2$ Disks Exposed to Gamma Fields at 150°C in: (a) $O_2$ + 60% Saturated Steam (Experiment C, Sample X); and (b) Ar+ 60% Saturated Steam (Experiment D, Sample V) | 9 |
| 5. | Valence Band Region in the XPS Spectra of $UO_2$ Disks Exposed to Gamma Fields at 150°C in: (a) $O_2$ + 60% Saturated Steam (Experiment C, Sample X); and (b) Ar + 60% Saturated Steam (Experiment D, Sample V) | 10 |
| 6. | Resolution of the U $4f_{7/2}$ Band into $U^{6+}$ and $U^{4+}$ Components for $UO_2$ Disks in Air: (a) Open Vial (Experiment A, Sample M); and (b) Vial Sealed with Air (Experiment B, Sample L) | 11 |
| 7. | XPS Spectrum for the O 1s Regions of a $UO_2$ Disk Exposed to Gamma Fields at 150°C in Air (Open Vial, Experiment A, Sample M) | 12 |
| 8/1: | XRD Patterns of $UO_2$ Disk Surfaces Subjected to Gamma Fields at 150°C in: (a) Vials Open to the Atmosphere of the Vessel (Experiment A, Sample M); (b) Vials Sealed with Air (Experiment B, Sample L) | 14 |
| 8/2: | XRD Patterns of $UO_2$ Disk Surfaces Subjected to Gamma Fields at 150°C in: (c) Sealed Vials, $O_2$ + 60% Saturated Steam (Experiment C, Sample X) and; (d) Vials Sealed with Ar + 60% Saturated Steam (Experiment D, Sample V) | 15 |


continued...

LIST OF FIGURES (concluded)


| | | Page |
|---|---|---|
| 9/1: | XRD Patterns, for 2θ Region Between 15-40° of $UO_2$ Disk Surfaces in: (a) Vials Open to the Atmosphere of the Vessel (Experiment A, Sample M); (b) Vials Sealed with Air (Experiment B, Sample L) | 16 |
| 9/2: | XRD Patterns, for 2θ Region Between 15-40° of $UO_2$ Disk Surfaces in: (c) Sealed Vials, $O_2$ + 60% Saturated Steam (Experiment C, Sample X) and; (d) Vials Sealed with Ar + 60% Saturated Steam (Experiment D, Sample V) | 17 |
| 10: | XRD Patterns, for 2θ Region Between 15-40° of $UO_2$ Disk Surfaces in Vials Sealed with Ar + 60% Saturated Steam (Experiment D): (a) Sample V and (b) Sample O (with $O_2$ Impurity?) | 18 |
| 11. | XRD Patterns, for 2θ Region Between 54-60°, of $UO_2$ Disk Surfaces in Vials Sealed with Ar + 60% Saturated Steam (Experiment D): (a) Sample V; and (b) Sample O (with $O_2$ Impurity?) | 21 |
| 12. | Lower Magnification SEM Micrographs of $UO_2$ Disk Surfaces in: (a) Vials Open to the Atmosphere of the Vessel (Experiment A, Sample M); (b) Vials Sealed with Air (Experiment B, Sample L); (c) Sealed Vials, $O_2$ + 60% Saturated Steam (Experiment C, Sample X); and (d) Vials Seals with Ar + 60% Saturated Steam (Experiment D, Sample V) | 22 |
| 13. | Higher Magnification SEM Micrographs of $UO_2$ Disk Surfaces in: (a) Vials Open to the Atmosphere of the Vessel (Experiment A, Sample M); (b) Vials Sealed with Air (Experiment B, Sample L); (c) Sealed Vials, $O_2$ + 60% Saturated Steam (Experiment C, Sample X); and (d) Vials Sealed with Ar + 60% Saturated Steam (Experiment D, Sample V). These samples are the same as used in Figure 12 | 23 |
| A-1: | Schematic of Locations Used for Calculating Dose Rate: A, Centre of Fuel Vessel; B, Centre of Aluminum Vessel Containing $UO_2$ Samples (see Figure 3); and T, Top of the Aluminum Vessel. T and T' are Locations of Dose Rate Measurements (see text). | 37 |

# 1. INTRODUCTION

Dry storage of used nuclear fuel in above-ground containers offers an economical option for short- to medium-term storage until a permanent disposal facility becomes available. Used fuel is already being stored in concrete canisters at several Canadian reactor sites [1-5 and references therein].

The performance of used CANDU[1] fuel in a dry-storage facility will be affected by the extent of air oxidation of any defected fuel bundles. Oxidation of $UO_2$ fuel to $U_3O_8$ (or $UO_3$) results in a volume expansion [6] that could cause powdering of the fuel and splitting of the Zircaloy cladding. Therefore, the oxidation of used fuel bundles with deliberately introduced defects, at somewhat higher than anticipated storage temperatures, is being investigated at Whiteshell Laboratories [3-5]. These are called "Controlled Environment Experiments" (CEX). The CEX-1 experiment is investigating the storage of used fuel in dry air, while the CEX-2 experiment is investigating storage in moisture-saturated air. Both are being conducted at 150°C. The results from CEX-1 were used to develop a model for predicting the progress of oxidation of defected fuel elements in a dry-storage facility [7]. This model predicted that the oxygen in the storage container would be consumed very rapidly, at a rate about two orders of magnitude larger than the rate calculated using literature data on $UO_2$ oxidation. To resolve this discrepancy, it is necessary to have accurate data on fuel oxidation.

The radioactivity associated with used fuel samples [8] limits the handling and analysis of the samples to determine the extent of oxidation. One must use small samples of used fuel to reduce the exposure of operator and equipment to radiation [5,9]. Therefore, we have studied the oxidation of unirradiated CANDU fuel exposed to selected controlled atmospheres at ~150°C in gamma fields equivalent to those associated with used CANDU fuel. These studies complement the air oxidation studies of irradiated CANDU fuel [3-5] and of unirradiated fuel without any applied gamma fields [1,6,10-14], being carried out at Whiteshell Laboratories. The results of these investigations are presented here.

# 2. EXPERIMENTAL

## 2.1 MATERIALS

$UO_2$ samples were obtained from an unused CANDU fuel bundle. The fuel pellets consist of sintered polycrystalline $UO_2$, with a density of ~10.6 $g \cdot cm^{-3}$, i.e., > 96% of theoretical density. The pellets (diameter 13 mm) were cut into ~3 mm-thick disks using a diamond saw. The estimated weight of the disks was ~4 g each.

The disks were mechanically polished on all sides, including the rim, using 600-grit SiC paper, to expose a fresh $UO_2$ surface [15]. An identifying letter was engraved on the bottom face of each disk to distinguish between samples. The disks were stored in an inert atmosphere glovebox prior to being sealed in specially designed glass vials to minimize oxidation by atmospheric $O_2$.

---

[1]CANada Deuterium Uranium, registered trademark of AECL

Four types of experiments were carried out:

Type A: three glass vials (volume ~10 mL), each containing a ~4 g $UO_2$ disk, open to the atmosphere; Figure 1a.

Type B: three vials, same as Type A, except sealed under one atmosphere of air at room temperature; Figure 1b.

Type C: three vials, same as Type A, except sealed under one atmosphere of $O_2$ (at room temperature) and containing 0.015 g water to produce 60% saturated steam (ss) at 150°C; Figure 1c [16].

Type D: three vials, same as Type A, except sealed under one atmosphere of Ar (at room temperature) and containing 0.015 g water to produce 60% ss at 150°C; Figure 1c.

There was no water deliberately added to the vials used in Experiments A and B. The air sealed in the vials in Type B contained ambient humidity. The vials were constructed from ~20 mm o.d. Pyrex glass tubes, wall thickness 1.5 mm. The wide bottom ends of the vials were sealed after the polished disks were placed in the tubes. The narrow necks of the vials were left unsealed for Experiment A (Figure 1a) and sealed for Experiments B, C and D after the vials were purged with the desired gas (Figures 1b and 1c). For Experiments C and D, water was added to each vial, using a calibrated Eppendorf pipette attached to a thin Teflon tube, after purging with $O_2$ (Experiment C) or Ar (Experiment D) but before sealing the top end. The inner lip near the bottom of the vials used in Experiments C and D (Figure 1c) ensured that the $UO_2$ disks were not in direct contact with liquid water prior to heating.

The glass vials, containing polished $UO_2$ disks, were placed in a specially designed aluminum vessel, Figure 2. The vessel was placed in the central position between four vessels containing used CANDU fuel bundles, in a shielded canister in the Immobilized Fuel Test Facility (IFTF) at the Whiteshell Laboratories [5,17], Figure 3. Thus, $UO_2$ disks in the glass vials experienced essentially the same gamma field as did the used CANDU fuel bundles. The gamma field at the centre of the vials is estimated to be about 15 Gy/h, similar to that expected for 10- to 20-year old CANDU fuel (Appendix A). The temperature of the canister was raised to 150°C over a period of about 2 days. Power to the canister heater was turned off every three weeks to sample the atmosphere in the used fuel vessels. Downtime on each occasion was ~3 days. The $UO_2$ samples were exposed to this heating (3 weeks at 150°C) and cooling (3 days at ~30°C) cycle for 2.1 a, then retrieved.

The aluminum vessel containing the sample vials was removed from the IFTF canister after it had cooled down to room temperature and its outer surface was decontaminated. The glass vials, containing $UO_2$ disks, were checked for contamination and transferred into a nominally $O_2$-free, inert-atmosphere box. The sample disks were taken out of the glass vials by breaking the vials in the inert atmosphere box. They were then mounted on the XPS specimen holder and brought into the X-ray photoelectron spectrometer for analysis [15,18]. The surfaces of

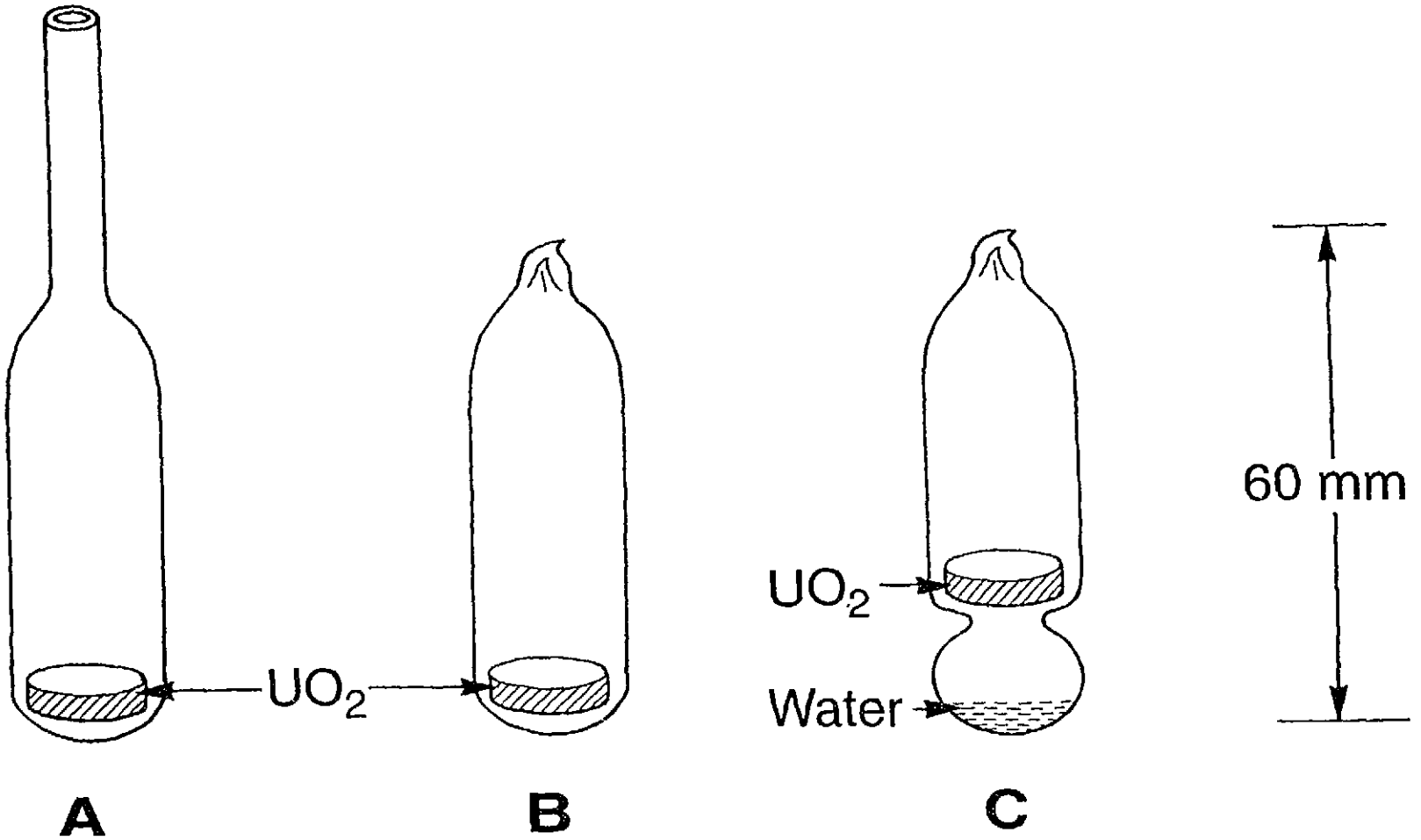


FIGURE 1: Schematic Diagrams of Glass Vials Used to Study Oxidation of $UO_2$ in Gamma Fields at High Temperatures: (a) Open to Atmosphere (Experiment A); (b) Sealed with Air (Experiment B); (c) Sealed with $O_2$ or Ar and Water (Experiments C and *D*)

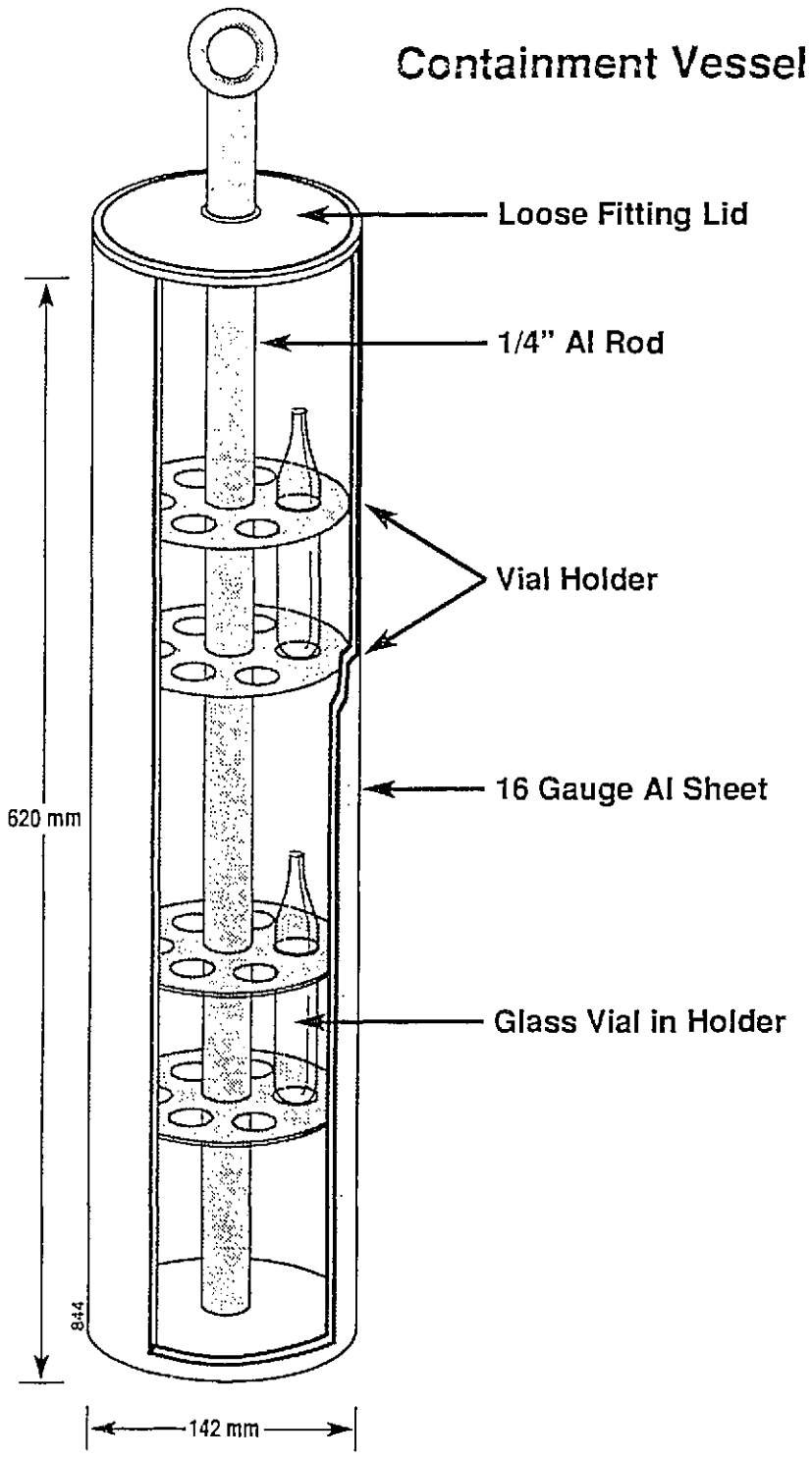


FIGURE 2: Schematic Diagram of Experimental Set-up (Vessel with $UO_2$ Vials)

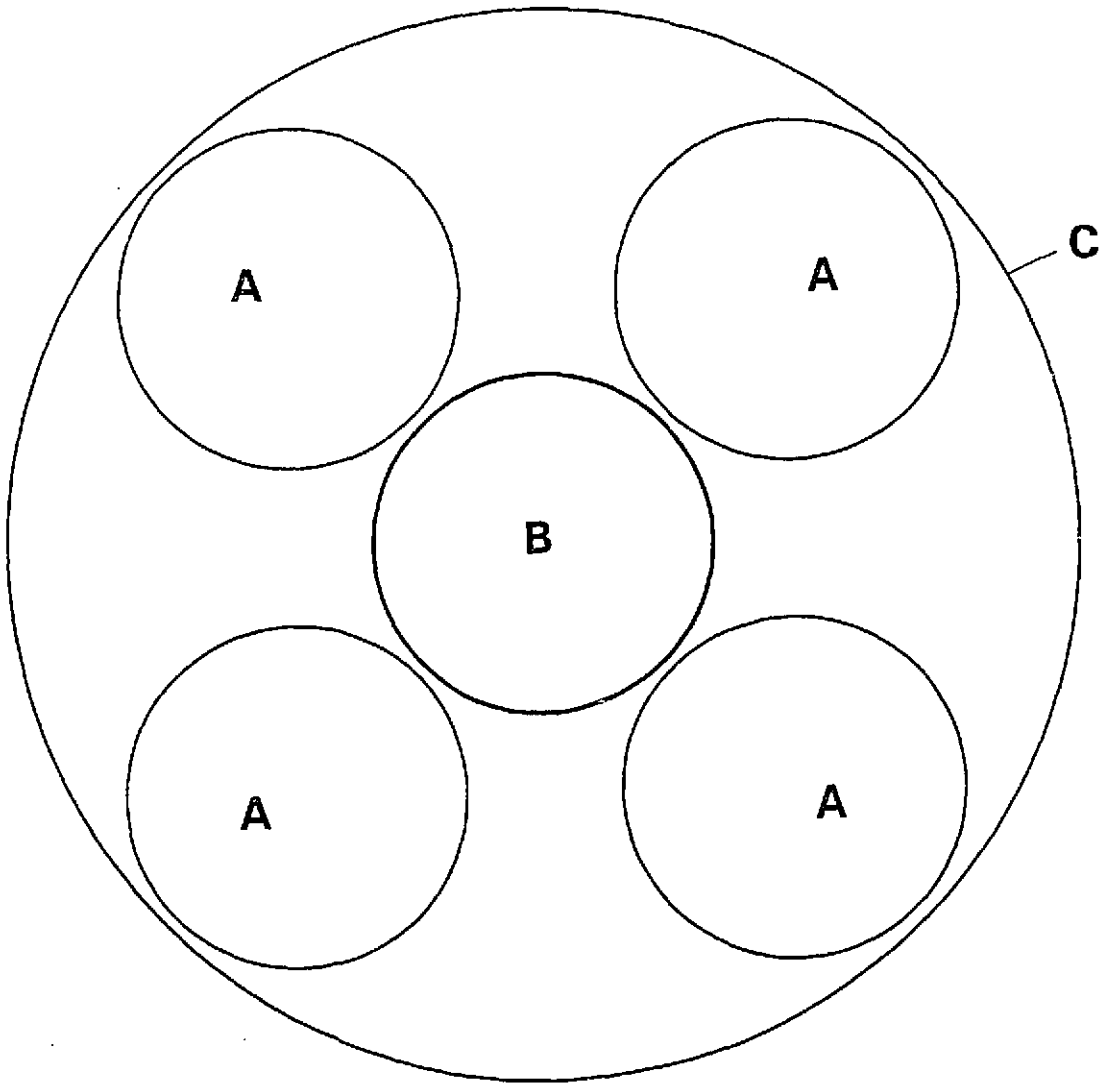


FIGURE 3: Schematic Diagram of the Relative Placement of the Vessels Containing $UO_2$ Samples and Used CANDU Fuel: A, Used Fuel Container; B, $UO_2$ Container; and C, IFTF Canister

the disks were analyzed using X-ray photoelectron spectroscopy (XPS), X-ray diffraction (XRD) and scanning electron microscopy (SEM), in that order.

## 2.2 X-RAY PHOTOELECTRON SPECTROSCOPY

The XPS studies were carried out using a PHI-5300 ESCA system, which allows one to transfer samples from the inert atmosphere chamber to the evacuated sample compartment of the XPS spectrometer without exposure to air using a vacuum transfer vessel [18]. The XPS spectra were excited using Mg Kα radiation filtered through an Al window. The energy scale of the spectrometer was calibrated using the following line positions of noble metals: Au $4f_{7/2}$, 84.0 eV; Ag $3d_{5/2}$, 368.3 eV; and Cu $2p_{3/2}$, 932.56 eV [19-21].

## 2.3 X-RAY DIFFRACTION

After XPS analysis, XRD data were obtained from the complete sample disks, using a Rigaku Rotaflex X-ray diffractometer equipped with a 12-kW rotating-anode Cu Kα X-ray source and a diffracted-beam graphite monochromator. The diffractometer was calibrated using a silicon standard from the U.S. National Bureau of Standards (NBS)[2]. The diffractometer scanning rate was $1°(2\theta)\cdot min^{-1}$. The data were acquired using a Rigaku IBM PC (Version 3.0, June 1992) data acquisition system and analyzed using JADE+ software obtained from Material Data Inc. of Livermore, CA, U.S.A.

## 2.4 SCANNING ELECTRON MICROSCOPY

The sample surfaces were examined using a JEOL JSM-6300V scanning electron microscope after XRD analysis. The microscope was equipped with a $LaB_6$ electron gun. The micrographs were recorded using an accelerating voltage of 15 kV, beam diameter ~50 μm, and sample current ~4 pA. The specimens were gold-coated to minimize surface charging.

# 3. RESULTS AND DISCUSSION

## 3.1 VISUAL OBSERVATIONS

All disks were recovered intact from the vials. In Experiment D (Ar + water), water droplets were found on the surface of the disks as well as on the inner walls of the glass vials at the end of the Experiment; we thus conclude that there were no leaks in these vials. The disks used in Experiment C ($O_2$ + 60% ss) were generally darker in colour than the other disks. One of the sample disks in Experiment C (labelled X in Table 1) had a slight yellowish surface coloration.

---

[2] The present name of the NBS is National Institute of Standards and Technology (NIST)

TABLE 1

XPS RESULTS FOR THE SURFACE OXIDATION OF $UO_2$ DISKS AT 150°C IN GAMMA FIELDS

| Experiment Type | Atmosphere[a] | Sample # | XPS Results | | |
|---|---|---|---|---|---|
| | | | $U^{6+}/U^{4+}$ Ratio | $U^{6+}$ % | $U^{4+}$ % |
| A | Air, open | M | 2.8 | 74 | 26 |
| | | N | 3.7 | 79 | 21 |
| | | S | 2.6 | 72 | 28 |
| B | Air, closed | L | 6.2 | 86 | 14 |
| | | P | 5.6 | 85 | 15 |
| | | Q | 10 | 91 | 9 |
| C | $O_2$ + 60% ss | W | 11 | 92 | 8 |
| | | X | 118 | 99 | 1 |
| | | Z* | 2.2 | 69 | 31 |
| D | Ar + 60% ss | V Top | 0.01 | 1 | 99 |
| | | Bottom | 0.02 | 2 | 98 |
| | | U Top | 0.01 | 1 | 99 |
| | | Bottom | 0.01 | 1 | 99 |
| | | O** Top | 0.30 | 23 | 77 |
| | | Bottom | 0.40 | 28 | 72 |

[a] ss means saturated steam at 150°C.

* This Experiment's atmosphere was probably equivalent to A (see text).

** This sample's atmosphere probably contained a trace of $O_2$ impurity (see text).

## 3.2 X-RAY PHOTOELECTRON SPECTROSCOPY

Low-resolution survey spectra were recorded for the 0- to 1100-eV region to determine the elements present in the sample surface and to check for surface contamination.
High-resolution spectra were recorded for the U 4f, valence bands (0-20 eV), O 1s and C 1s regions to determine the chemical state of these elements (the carbon signal was due to ubiquitous hydrocarbons present on solid surfaces). The C 1s band was used to correct for charging with a binding energy value of 284.8 eV for this peak [15].

The band due to the U $4f_{7/2}$ core level is very sensitive to the chemical state of the uranium atoms, and can be quantitatively resolved into $U^{6+}$ and $U^{4+}$ components to determine their relative amounts in the XPS sample, as described in references 20, 22 and the references therein. The relative area of the $U^{6+}$ and $U^{4+}$ peaks is a direct measure of the oxidation state of the uranium atoms in the sample surface. Results obtained from the analysis of the U $4f_{7/2}$ band were verified by analyzing the relative intensities of the bands in the valence region [20,22-24]. A $U^{4+}$ atom has two electrons in its 5f valence shell. The band seen around 1 eV in the XPS spectra of uranium compounds is assigned to these electrons [15,20,23-25]. Oxidation of $U^{4+}$ compounds, e.g., $UO_2$, results in the loss of these electrons from the uranium atom and is indicated in the spectrum by a decrease in the intensity of this band. Intensity measurements are not affected by any error in the binding energy scale, and thus provide an independent check on the results from the analysis of the U $4f_{7/2}$ band.

Figures 4 and 5 show the spectra for the U 4f and valence regions, respectively, for one sample each from Experiment C (sealed vials, $O_2$ + 60% ss, sample X) and Experiment D (sealed vials, Ar + 60% ss, sample V). The spectra shown in Figures 4a and 5a are typical of those observed for $U^{6+}$ oxides, i.e., $UO_3$, [24,26] while the spectra shown in Figures 4b and 5b are typical of those seen for $U^{4+}$ oxides, i.e., $UO_2$ [23,24,27]. Thus, the U 5f band has high intensity in the spectrum of sample V, Figure 5b, while it shows very little intensity in the spectrum of sample X, Figure 5a. Deconvolution of the U $4f_{7/2}$ band into $U^{6+}$ and $U^{4+}$ components indicates that the band for sample X (Experiment C) can be accounted for mainly by a $U^{6+}$ feature ($U^{6+}/U^{4+}$ ratio ~100), while that for sample V, (Experiment D) can be accounted for primarily by a $U^{4+}$ feature ($U^{6+}/U^{4+}$ ratio ~0.01), Table 1. The U $4f_{7/2}$ bands in the XPS spectra of one sample from Experiment A (sample M) and one sample from Experiment B (sample L) are analyzed in Figure 6. These spectra yielded $U^{6+}/U^{4+}$ ratios of ~2.8 and 6.2, respectively.

Table 1 gives all the XPS results, expressed as uranium oxidation states, obtained by analyzing the U $4f_{7/2}$ band. In all samples exposed to air or $O_2$ (Experiments A, B and C) the $U^{6+}/U^{4+}$ ratio is $\geq 2$, indicating that the surface of these samples has been oxidized to phase(s) with average oxidation state(s) equal to or higher than that in $U_3O_8$ (the $U^{6+}/U^{4+}$ ratio is equal to 2 in $U_3O_8$). The highest ratios are seen for Experiment C ($O_2$ + 60% ss), Table 1. The surface of sample X, as seen by XPS, contains uranium almost entirely in the +6 state. In contrast, the samples exposed to water vapour radiolysis at 150°C in $O_2$-free atmosphere (samples U and V, Table 1) appear to have undergone no oxidation. To confirm this observation, we analyzed both faces of the sample disks used in Experiment D (samples U, V and O). Both faces of disks U and V show no oxidation. However, one of the samples in Experiment D, disk O, shows some oxidation, i.e., $U^{6+}/U^{4+}$ ratios of 0.3 and 0.4 for its two faces. These values are less than the value of 0.5 expected for $U_3O_7$. We believe that the slight oxidation suffered by this sample is probably due to the presence of traces of $O_2$ impurity, which could have entered the vial during the glass-sealing step.

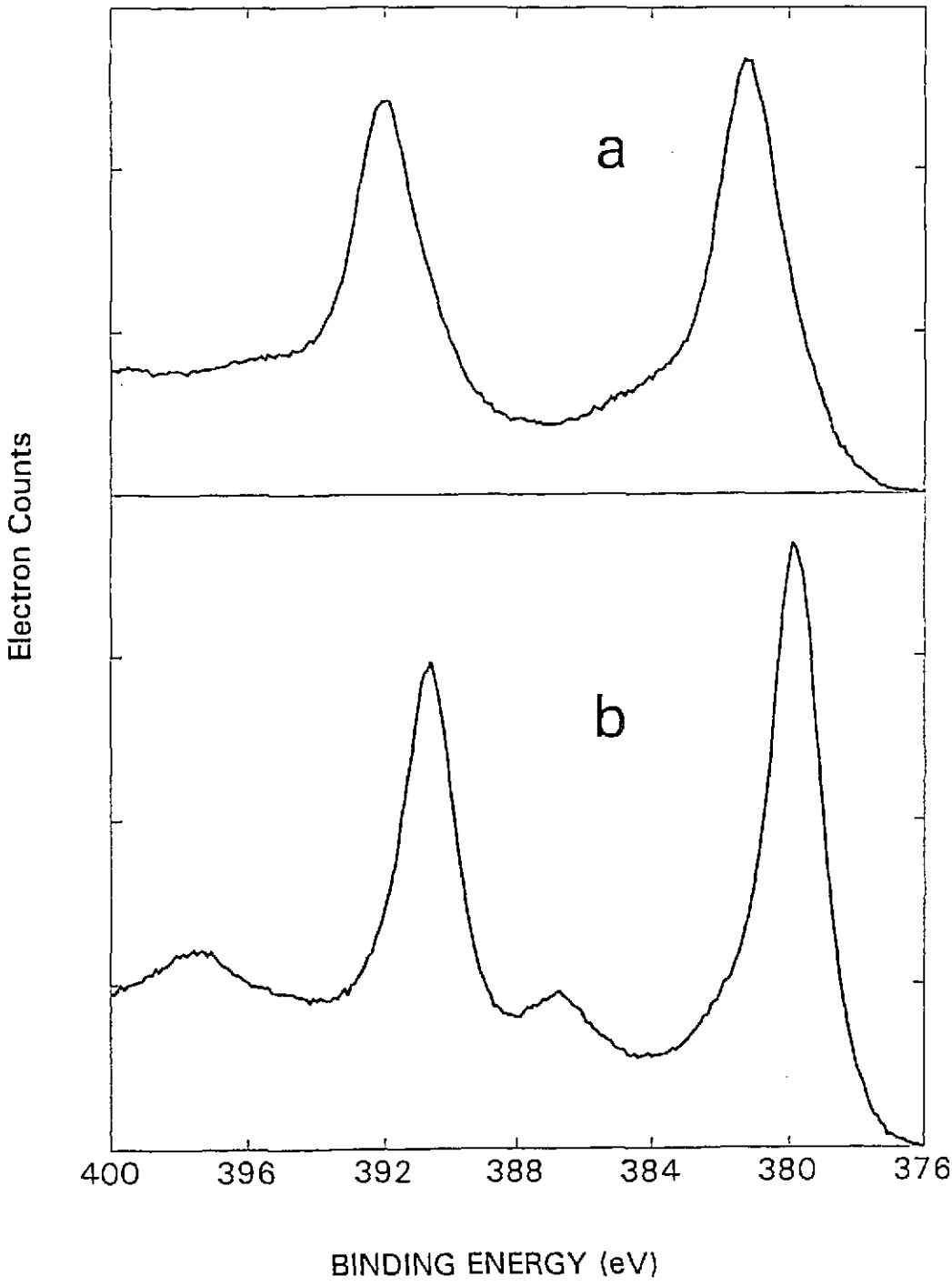


FIGURE 4: XPS Spectra for the U 4f Region of $UO_2$ Disks Exposed to Gamma Fields at 150°C in: (a) $O_2$ + 60% Saturated Steam (Experiment C, Sample X); and (b) Ar+ 60% Saturated Steam (Experiment D, Sample V)

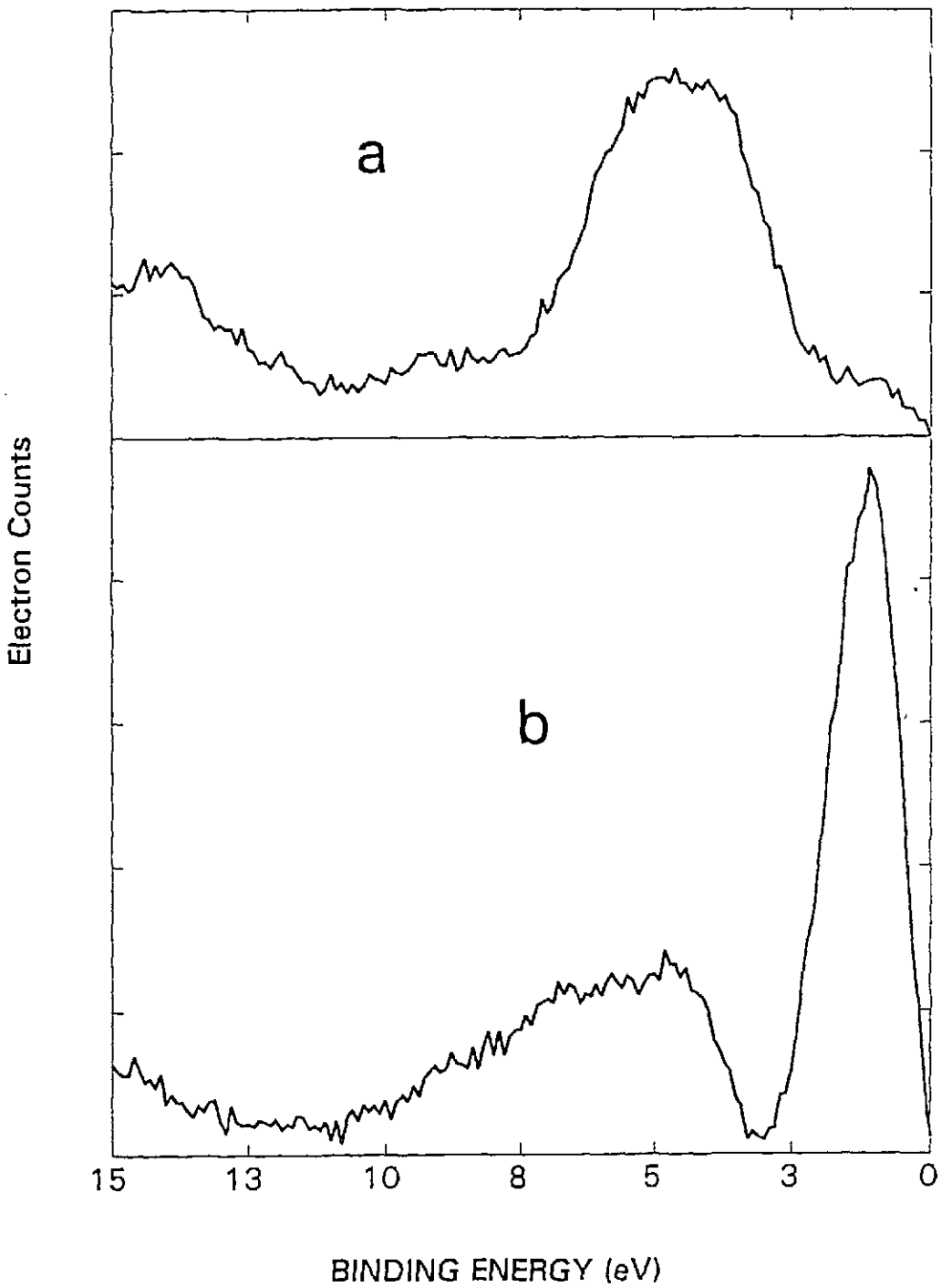


FIGURE 5: Valence Band Region in the XPS Spectra of $UO_2$ Disks Exposed to Gamma Fields at 150°C in: (a) $O_2$ + 60% Saturated Steam (Experiment C, Sample X); and (b) Ar + 60% Saturated Steam (Experiment D, Sample V)

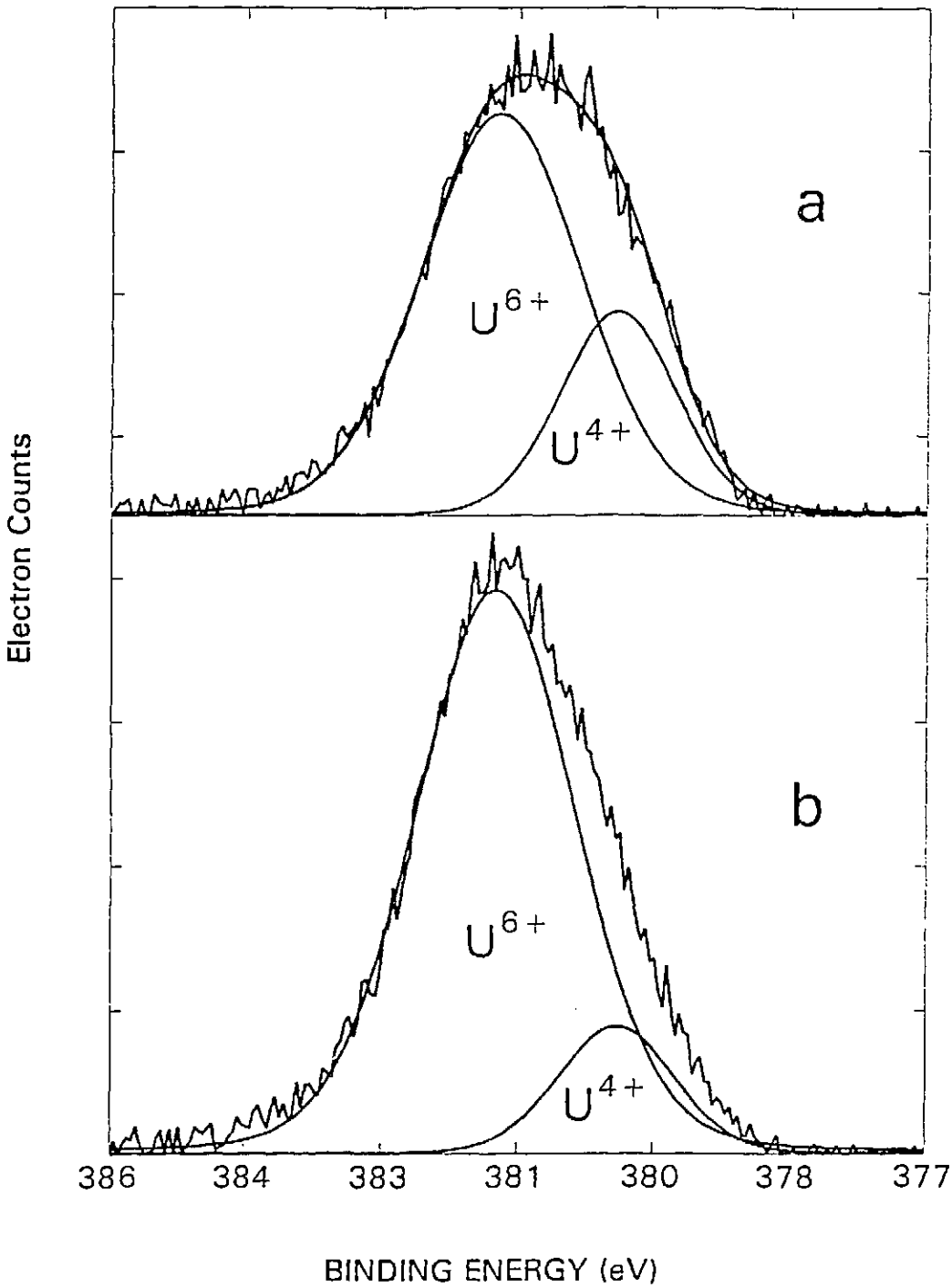


FIGURE 6: Resolution of the U $4f_{7/2}$ Band into $U^{6+}$ and $U^{4+}$ Components for $UO_2$ Disks in Air: (a) Open Vial (Experiment A, Sample M); and (b) Vial Sealed with Air (Experiment B, Sample L)

The $U^{6+}/U^{4+}$ ratio for one of the samples in Experiment C, sample Z, is significantly lower than those observed for the other two samples in this Experiment (Table 1). The $U^{6+}/U^{4+}$ ratio for this sample is similar to those observed for the samples used in Experiment A (open air). One possible explanation for this result is that the glass vial for this sample may have contained a leak, resulting in the loss of water on heating and rendering the Experiment equivalent to type A (open air) rather than type C ($O_2$ + 60% ss). The XRD results for this sample are in agreement with these XPS results (see below).

The $U^{6+}/U^{4+}$ ratios are higher in Experiment B (air-sealed vials) than Experiment A (open vials) even though the air ($O_2$) available to the samples in Experiment A was nominally unlimited. The XRD results are consistent with this observation (see below).

The O 1s spectra of all the samples indicate the presence of both metal-oxide ($O^{2-}$) and hydroxyl and water species in the sample surfaces, as illustrated in Figure 7 for sample M (Experiment A). The procedure to resolve the O 1s band into $O^{2-}$, $OH^-$ and $H_2O$ components has been discussed elsewhere [20,28]. All the samples showed the presence of $OH^-$ and $H_2O$ features, in addition to the $O^{2-}$ feature, in the O 1s band in the XPS spectra.

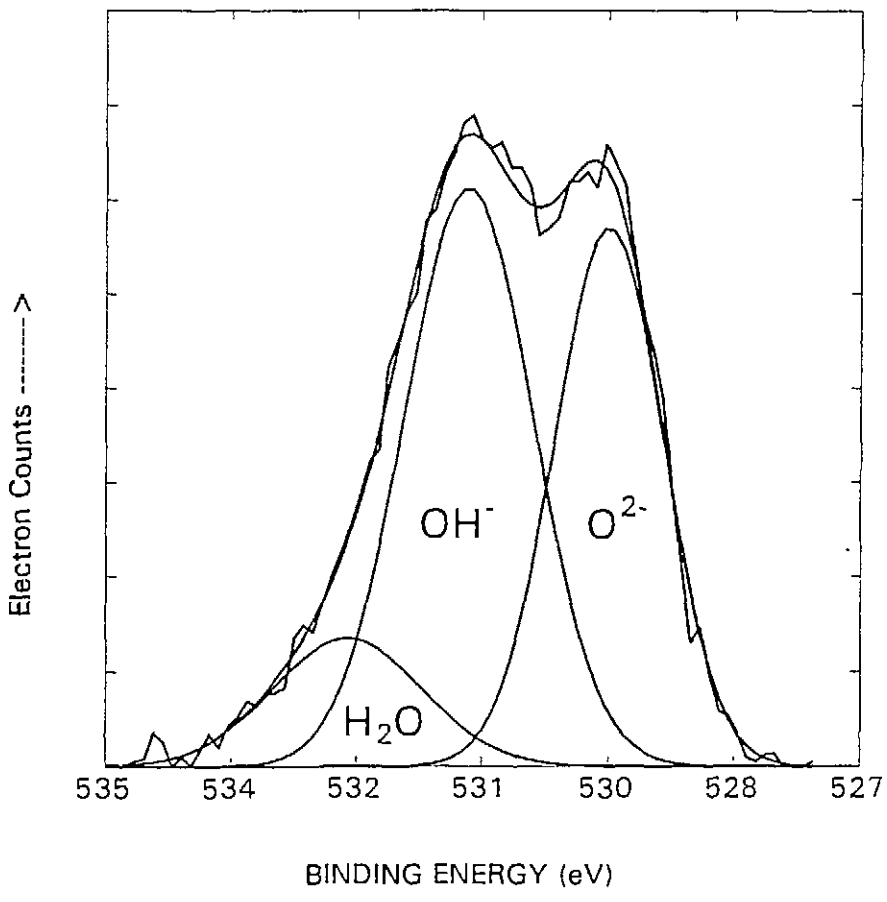


FIGURE 7: XPS Spectrum for the O 1s Region of a $UO_2$ Disk Exposed to Gamma Fields at 150°C in Air (Open Vial, Experiment A, Sample M)

## 3.3 X-RAY DIFFRACTION

X-ray patterns were recorded for the 2θ range between 10 and 120°. XRD patterns were not recorded for sample U, which (like sample V) experienced no oxidation according to the XPS results discussed above (Table 1).

The use of XRD to detect the products formed on $UO_2$ surfaces during oxidation has been described by several authors [e.g. references 10,12,13,29-32]. Because the unit cells of $U_4O_9$ and $U_3O_7$ are similar to that of $UO_2$, the oxidation of $UO_2$ to $U_4O_9/U_3O_7$ results mainly in the distortion and/or displacement of the XRD features [10,29-34]. $UO_2$ has a cubic unit cell with $a$ = 5.4701 Å, while $U_4O_9$ also has a cubic unit cell with $a$ only slightly shorter than in $UO_2$ (5.44 Å); and the three $U_3O_7$ phases (α, β and γ) have tetragonal unit cells with $c/a$ values very close to 1 and with $a$ very close to that in $UO_2$ [30]. In contrast, oxidation to $U_3O_8$ or beyond (e.g., $UO_3$) causes the appearance of quite distinct features due to major changes in unit cell size and symmetry in going from $UO_2$ to $U_3O_8$ (or $UO_3$) [6,11,12,27,29,30,35]. Thus, the formation of $U_3O_8$ on $UO_2$ samples is easily detected in XRD by the appearance of characteristic 001 and 130/200 features of $U_3O_8$, with $d$ values of ~0.415 nm and 0.34 nm, respectively, (i.e., 2θ values of ~21° and ~26°, respectively, for CuKα X-rays).

Figure 8 shows XRD patterns of representative samples from the four types of Experiments in the present study. The $d$ spacings obtained from the XRD patterns shown in Figure 8 are listed in Appendix B. Figure 9 shows the region expected to contain the distinctive features of $U_3O_8$ (15 to 40°) on an expanded scale. The samples exposed to air or $O_2$ show the characteristic features attributed to $U_3O_8$ (see a, b and c in Figures 8 and 9). The 001 feature of $U_3O_8$ ($d$ ~ 0.415 nm, 2θ ~ 21°) is very intense in the XRD patterns of samples heated in air (Experiments A and B), Figures 8 and 9. This feature has the highest peak height in the XRD patterns of samples in Experiment B (closed vials containing air). The disproportionately high intensity of this feature is probably related to the preferential growth of $U_3O_8$ in the (001) direction on $UO_2$ grains with a (111) orientation [13,27,35]. The XRD patterns of the samples exposed to $O_2$+60% ss (Experiment C) are dominated by $UO_3 \cdot xH_2O$ phases, Figures 8c and 9c. In contrast, the samples exposed to Ar and $H_2O$, (Experiment D) including sample O, do not show these characteristic features of $U_3O_8$ in their XRD scans (Figures 9a and 10a).

Crystalline phases present in the surface of the samples were identified using the JADE+ computer software by phase matching with the powder diffraction patterns in the files of the Joint Committee for Powder Diffraction Standards [36]. Table 2 lists the major and minor uranium oxide phases identified by their XRD patterns. It should be noted that the major phases present in the surface of samples W and X, Experiment C ($O_2$ + 60% ss), are uranium trioxides, i.e., U oxidation has gone beyond the $U_3O_8$ stage, a result consistent with the XPS results for the two samples (Table 1).

One can estimate the fraction of $U_3O_8$ present in the surface of a $UO_2$ sample subjected to oxidation from the relative intensities of the characteristic features in the XRD patterns of $UO_2/U_3O_7$ and $U_3O_8$ using a procedure recently developed by Choi et al. [37]. According to these authors:

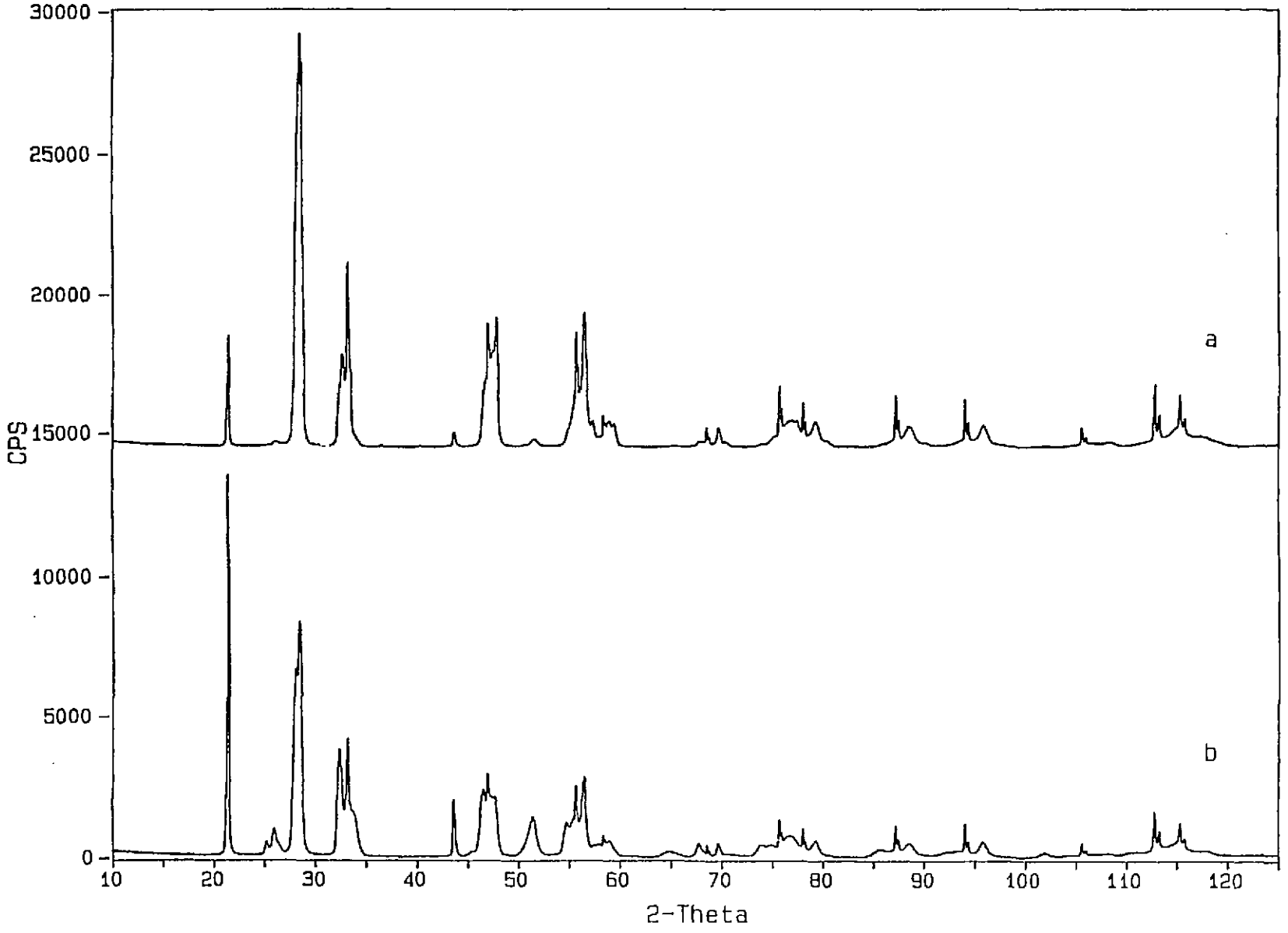


FIGURE 8/1: XRD Patterns of $UO_2$ Disk Surfaces Subjected to Gamma Fields at 150°C in: (a) Vials Open to the Atmosphere of the Vessel (Experiment *A*, Sample *M*); (b) Vials Sealed with Air (Experiment *B*, Sample *L*)

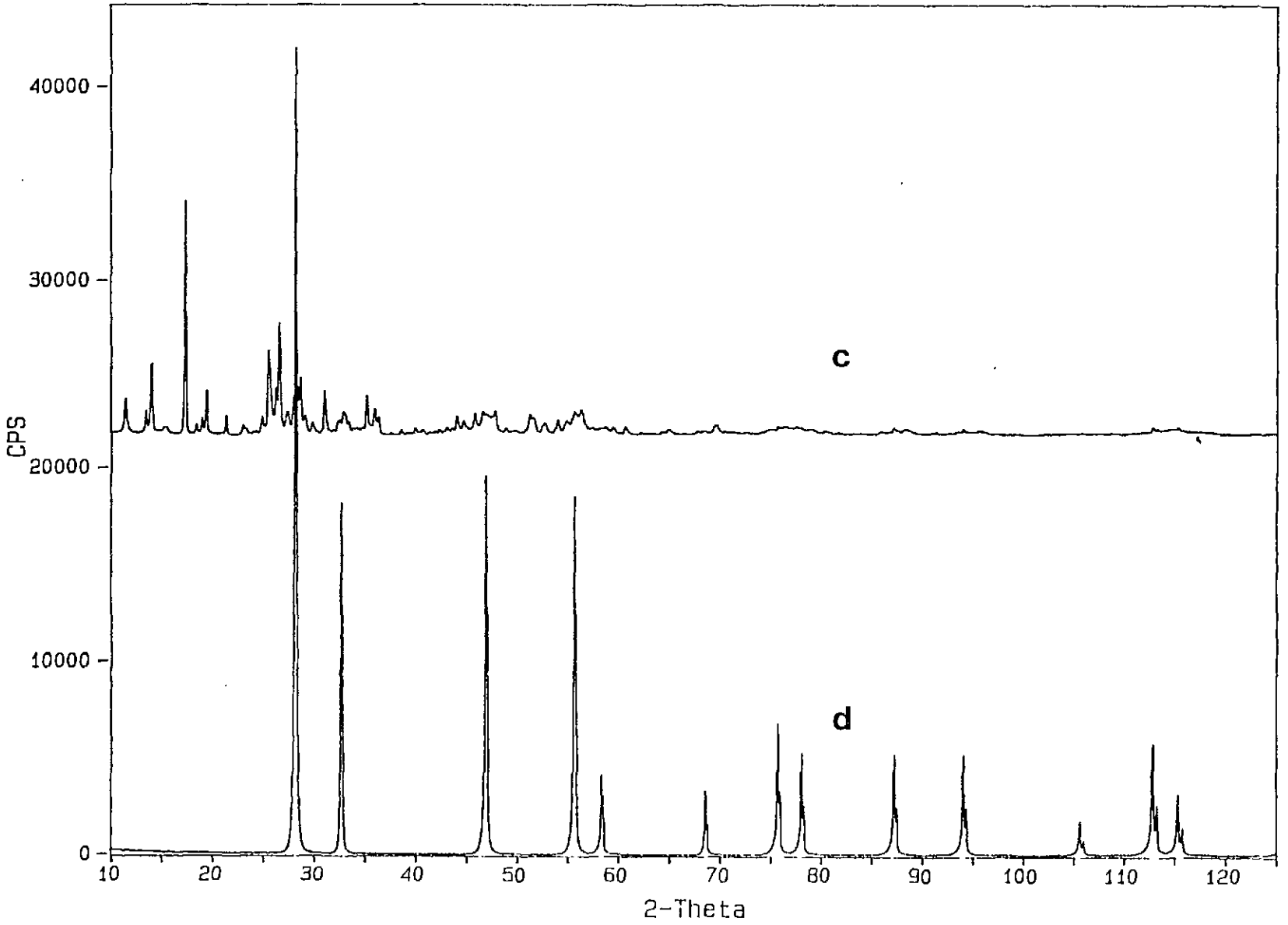


FIGURE 8/2: XRD Patterns of $UO_2$ Disk Surfaces Subjected to Gamma Fields at 150°C in: (c) Sealed Vials, $O_2$ + 60% Saturated Steam (Experiment C, Sample X) and; (d) Vials Sealed with Ar + 60% Saturated Steam (Experiment D, Sample V)

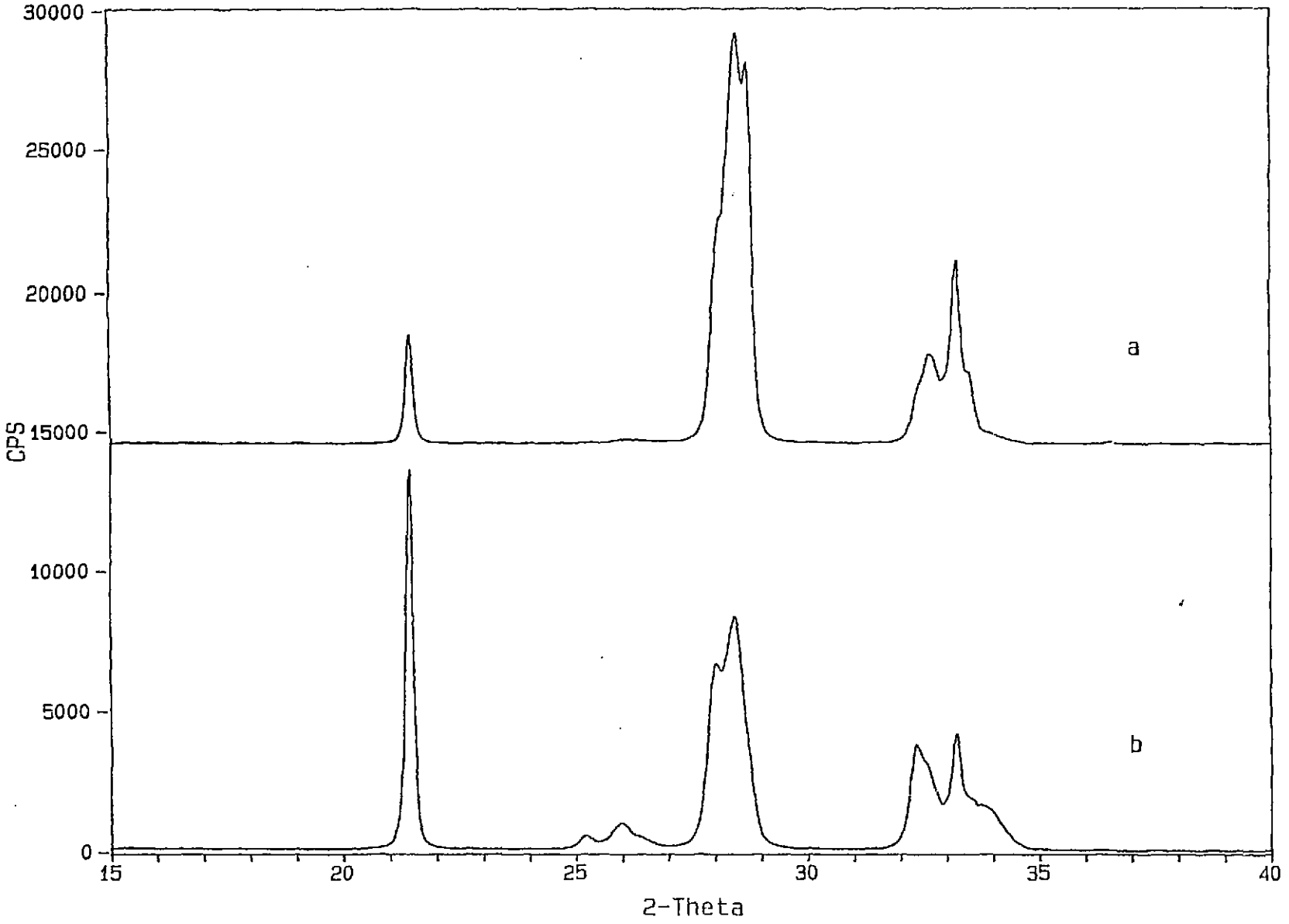


FIGURE 9/1: XRD Patterns, for 2θ Region Between 15-40° of $UO_2$ Disk Surfaces in: (a) Vials Open to the Atmosphere of the Vessel (Experiment A, Sample M); (b) Vials Sealed with Air (Experiment B, Sample L)

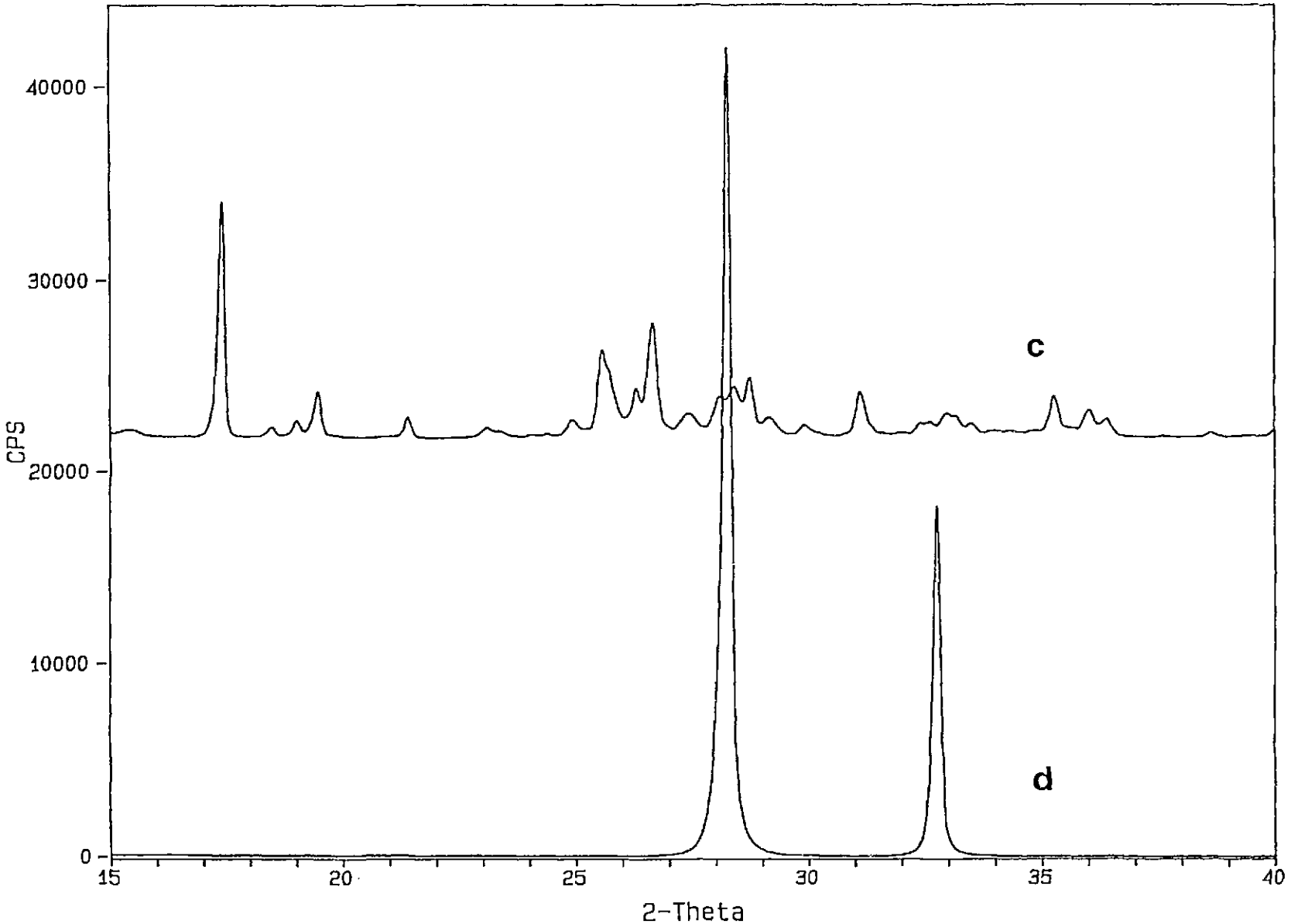


FIGURE 9/2: XRD Patterns, for 2θ Region Between 15-40° of $UO_2$ Disk Surfaces in: (c) Sealed Vials, $O_2$ + 60% Saturated Steam (Experiment C, Sample X) and; (d) Vials Sealed with Ar + 60% Saturated Steam (Experiment D, Sample V)

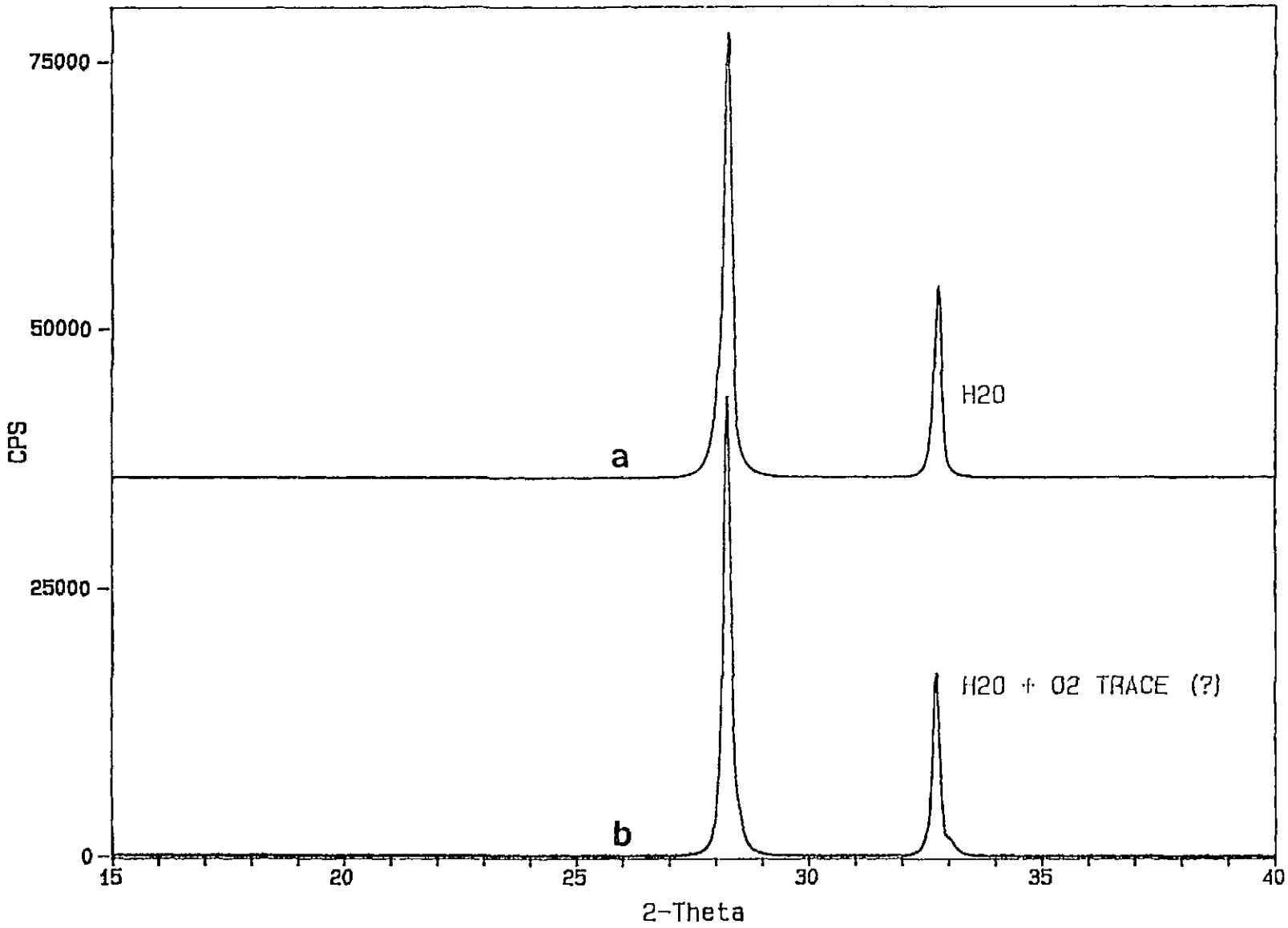


FIGURE 10: XRD Patterns, for 2θ Region Between 15-40° of $UO_2$ Disk Surfaces in Vials Sealed with Ar + 60% Saturated Steam (Experiment D): (a) Sample V and (b) Sample O (with $O_2$ Impurity?)

TABLE 2

COMPARISON OF XPS AND XRD ANALYSIS OF

THE SURFACE OXIDATION OF $UO_2$ DISKS AT 150°C IN GAMMA FIELDS

| Experiment Type | Atmosphere* | Sample # | XPS Results | XRD Results |
|---|---|---|---|---|
| | | | $U^{6+}/U^{4+}$ Ratio | Oxide Phases Seen[a] |
| A | Air, open | M | 2.8 | $UO_2$, $U_3O_7$, $U_3O_8$, $U_8O_{19}$ |
| | | N | 3.7 | $UO_2$, $U_3O_7$, $U_3O_8$, $U_8O_{19}$ |
| | | S | 2.6 | $UO_2$, $U_3O_7$, $U_3O_8$, $U_8O_{19}$ |
| B | Air, closed | P | 5.6 | $UO_2$, $U_3O_7$, $U_3O_8$, $U_8O_{19}$ |
| | | Q | 10 | $UO_2$, $U_3O_7$, $U_3O_8$, $U_8O_{19}$ |
| | | L | 6.2 | $UO_2$, $U_3O_7$, $U_3O_8$, $U_8O_{19}$ |
| C | $O_2$ + 60% s.s. | W | 11 | $UO_2$, $U_3O_7$, $U_3O_8$, $UO_3$, $UO_3 \cdot xH_2O$, Soddyte |
| | | X | 118 | $UO_3 \cdot xH_2O$, $UO_3$, $U_3O_7$, Soddyte, $UO_2$, $U_3O_8$ |
| | | Z* | 2.2 | $U_3O_7$, $UO_2$, $U_3O_8$, $U_8O_{19}$, $UO_3$(?) |
| D | Ar + 60% s.s. | V | 0.01 | $UO_2$ |
| | | O* | 0.30 | $UO_2$, $U_3O_7$, $U_{16}O_{37}$ |

* See Footnotes under Table 1.

[a] The phases are listed in order of decreasing intensity in the XRD pattern.

$$F = I_1/(I_1 + \alpha I_o) \qquad (1)$$

where

$I_o$ = the integrated intensity of I11 features of $UO_2/U_3O_7$ (d ~0.31 mm and 2θ ~28.5°),

$I_1$ = the integrated intensity of 130 and 200 features of $U_3O_8$ (d ~0.34 mm and 2θ ~26°),

$\alpha$ = an empirical factor determined by Choi et al. with a value of 0.4504, and

F = the fraction of $U_3O_8$ in the XRD sampling depth (~1 to 3 μm)

Table 3 lists values of $I_0$, $I_1$ and F for all the samples investigated using XRD. Values of F are not included for samples W and X because, as noted above, the major surface phases were $UO_3$ hydrates. Major peaks from these phases overlap the 0.34 nm feature for $U_3O_8$, so that the calculation of F has no meaning in this situation.

The calculations of F consistently show that more $U_3O_8$ was formed in the sealed, nominally dry air environment (Experiment B) than in unlimited air (Experiment A). They also support the suggestion that vessel Z (Experiment C) was not leak-tight, and hence behaved like a Type A Experiment. Overall, these XRD results are consistent with the XPS findings.

The samples exposed to $H_2O$ and Ar atmosphere (samples V and O, Experiment D) show no sign of $U_3O_8$ formation (Figure 10, Table 3). Figures 10 and 11 compare the XRD patterns of these two samples for the 2θ regions from 15 to 40° and 55 to 60°, respectively. Both samples were nominally heated in Ar + 60% ss environment. The XPS results indicate slight oxidation of the surface of sample O (Table 1). The XRD pattern of sample V is identical to that expected for pure $UO_2$ [29,31,35], whereas the pattern of sample O shows the presence of small amounts of $U_4O_9/U_3O_7$ phases in the surface, as indicated by the appearance of weak shoulders on the high-angle side of the 200 ($d$ ~0.273 nm, 2θ ~32.8°), 311 ($d$ ~0.165 nm, 2θ ~55.8°) and 222 ($d$ ~0.157 nm, 2θ ~58.5°) peaks of uraninite [30,33], Figures 10 and 11.

## 3.4 SCANNING ELECTRON MICROSCOPY

The surface morphology of the samples, as seen in the SEM micrographs, is shown in Figures 12 and 13 (these micrographs are for the same samples whose XRD patterns are shown in Figures 8 and 9). Figure 13 gives a view at higher magnification of the samples. The surface of a sample exposed to the $H_2O$ + Ar atmosphere (sample V, Experiment D), Figures 12d and 13d, is typical of that seen for freshly polished, i.e., unoxidized $UO_2$. In contrast, the surface of a sample exposed to an atmosphere of $H_2O$ + $O_2$ is covered with crystals with a distinctly different morphology from the underlying matrix, indicating a surface recrystallization process, Figures 12c and 13c (sample X, Experiment C). This is consistent with the XPS and XRD results which indicate that this sample had undergone surface oxidation to hydrated $UO_3$ phases. The samples exposed to air (Experiments A and B) show some signs of surface alteration due to oxidation, Figures 12a, 12b, 13a and 13b.

## 3.5 DISCUSSION

The results presented here show that measurable quantities of $U_3O_8$ are formed on $UO_2$ disks exposed to air or $O_2$ at 150°C in the presence of gamma fields, comparable to those associated with 10- to 20-year old used fuel, in ~2.1 a. According to the information available, this is the first definitive observation of $UO_2$ oxidation by air or $O_2$ to $U_3O_8$ at such a low temperature. The formation of $U_3O_8$ by air or $O_2$ has been observed only in studies carried out at temperatures ≥ 200°C [13,27,35], most of which were carried out without any applied gamma fields. (Note that traces of $U_3O_8$ have been detected in the most recent examination of used CANDU fuel from the CEX-1 Experiment - irradiated $UO_2$ heated in air at 150°C for ~12 a [38].)

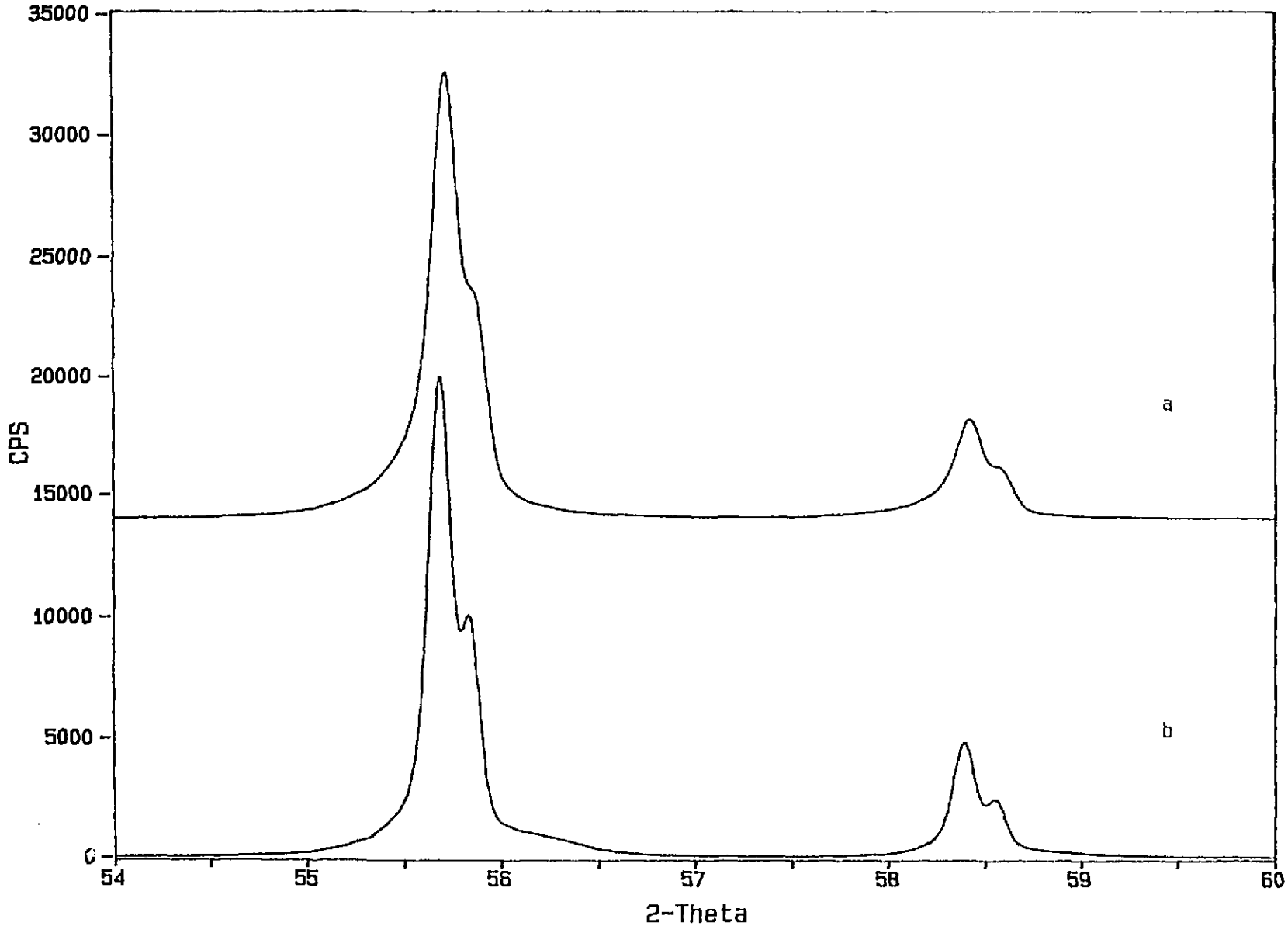


FIGURE 11: XRD Patterns, for 2θ Region Between 54-60°, of $UO_2$ Disk Surfaces in Vials Sealed with Ar + 60% Saturated Steam (Experiment D): (a) Sample V; and (b) Sample O (with $O_2$ Impurity?)

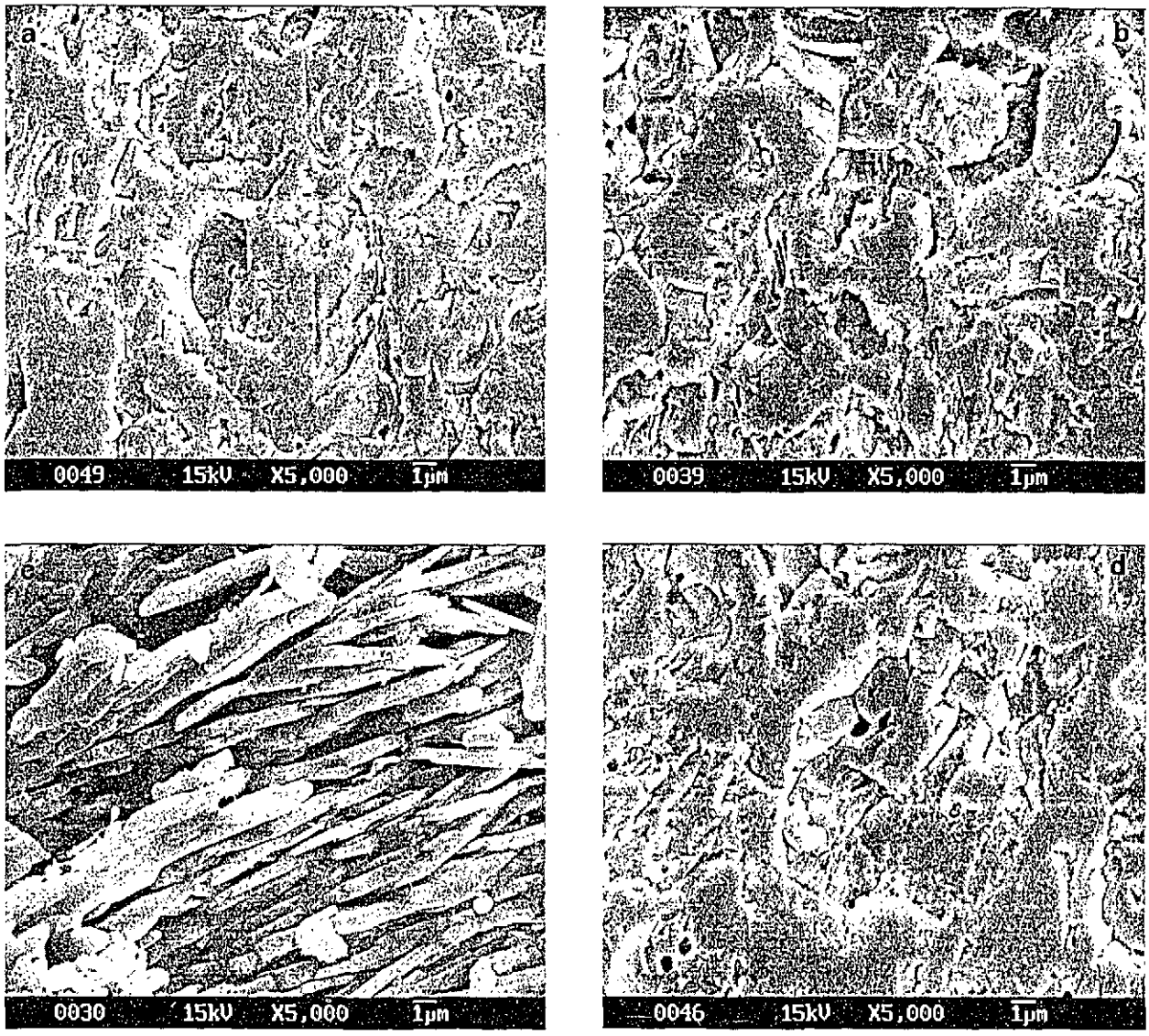


FIGURE 12: Lower Magnification SEM Micrographs of $UO_2$ Disk Surfaces in: (a) Vials Open to the Atmosphere of the Vessel (Experiment A, Sample M); (b) Vials Seals with Air (Experiment B, Sample L);; (c) Sealed Vials, $O_2$ + 60% Saturated Steam (Experiment C, Sample X); and (*d*) Vials Sealed with Ar + 60% Saturated Steam (Experiment D, Sample V)

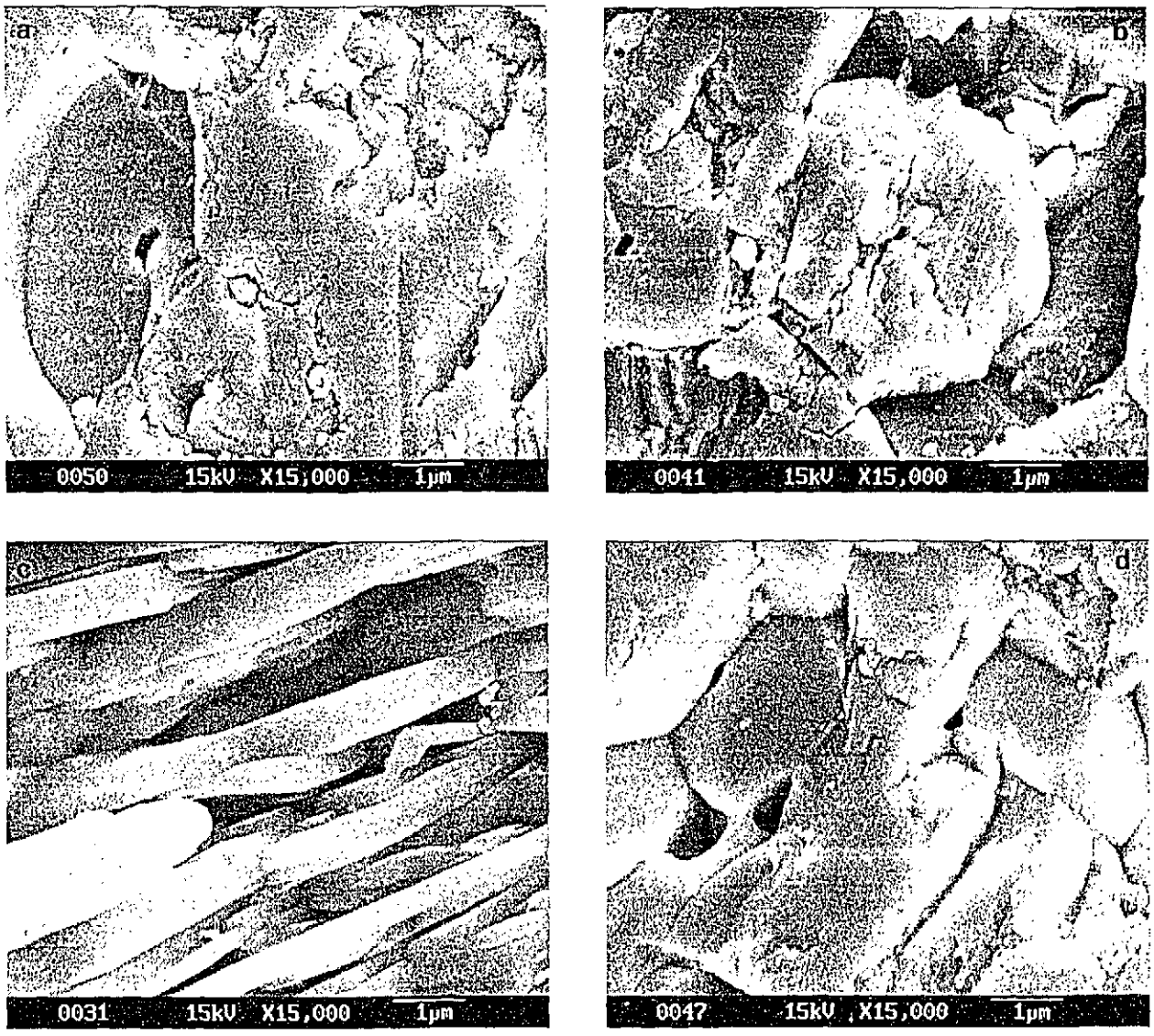


FIGURE 13: Higher Magnification SEM Micrographs of $UO_2$ Disk Surfaces in: (a) Vials Open to the Atmosphere of the Vessel (Experiment A, Sample M); (b) Vials Seals with Air (Experiment B, Sample L);; (c) Sealed Vials, $O_2$ + 60% Saturated Steam (Experiment C, Sample X); and (d) Vials Sealed with Ar + 60% Saturated Steam (Experiment D, Sample V). These samples are the same as used in Figure 12.

TABLE 3

CALCULATION OF FRACTION OF $U_3O_8$ FORMATION FROM XRD

| Experiment Type* | Sample | $I_o$ | $I_1$ | F |
|---|---|---|---|---|
| A | M | 17975 | 56 | 0.0069 |
| | N | 16941 | 48 | 0.0062 |
| | S | 17022 | 35 | 0.0045 |
| B | L | 10098 | 608 | 0.1179 |
| | P | 12977 | 518 | 0.0814 |
| | Q | 9860 | 647 | 0.1272 |
| C | W | 4992 | 4526 | ǂ |
| | X | 3169 | 2958 | ǂ |
| | Z* | 13340 | 28 | 0.0046 |
| D | V | 12329 | 0 | 0.0000 |
| | O* | 11007 | 0 | 0.0000 |

* See footnotes under Table 1.

$I_o$ = Intensity of 111 features of $UO_2/U_3O_7$.
$I_1$ = Intensity of 130/200 features of $U_3O_8$.
F = Fraction of $U_3O_8$ in surface calculated using Equation (1), see text.
ǂ = Not calculated due to interference from $UO_3 \cdot xH_2O$ phases.

Recently Taylor et al. have reviewed the literature on $U_3O_8$ formation by high temperature air oxidation of $UO_2$ and estimated times to reach three stages of formation of $U_3O_8$ at temperatures below 200°C [13]. The three stages of $U_3O_8$ formation refer to the amount of $UO_2$ oxidized to $U_3O_8$. The first stage refers to the formation of a detectable (by XRD) quantity of $U_3O_8$, the second stage refers to the formation of $U_3O_8$ as a minor surface phase (i.e., about 4 to 20% $U_3O_8$ in the surface layer probed by XRD), and the third stage refers to visible powder formation caused by oxidation of $UO_2$ to $U_3O_8$. They estimated the time needed to reach the first stage of $U_3O_8$ formation at 150°C as 1.9 a, which is close to 2.1 a, used in the present work (by coincidence the actual period at 150°C is ~1.9 a if one removes the cooling period from the heating-cooling cycle (see Section 2.1)). Also, the amount of $U_3O_8$ formed in Experiment A (open vials) is close to that expected for stage 1 of $U_3O_8$ formation, as described by Taylor et al. [13], Table 3.

Although $U_3O_8$ formation is seen in all the Experiments involving the heating of $UO_2$ in air/$O_2$ at 150°C in gamma fields (Experiments A, B and C), the amounts of $U_3O_8$ formed in the three Experiments are significantly different. Here we briefly discuss the possible causes

of these differences. The greater oxidation of $UO_2$ disks observed in closed air vials (Experiment B) than in open air (Experiment A), Table 1 and 3, at first seems unusual. One would have expected greater oxidation in samples of Experiment A, where the $O_2$ supply (from the air) was unlimited. The greater oxidation observed in Experiment B compared to that in Experiment A shows that the amount of available $O_2$ was not the limiting factor. The temperature, gamma fields and heating time were the same in all Experiments. However, pressure would be higher in the sealed vials at 150°C than in the open vials. (All vials were sealed with gas pressure of 1 atm at room temperature). Therefore, the increased oxidation observed in Experiment B (vials sealed with air) compared with Experiment A (open vials) is probably related to the higher partial pressure of oxidant(s) in the sealed vials.

It has been shown that the rate of $UO_2$ oxidation is essentially independent of $O_2$ pressure under the partial pressures of $O_2$ used in Experiments A and B [35,39,40]. Thus, it is unlikely that the increased oxidation observed in Experiment B was due to higher partial pressure of $O_2$ in the sealed vials. Therefore, we believe that the increased oxidation observed in Experiment B (vials sealed with air) compared with the Experiment A (open vials with air) is most probably due to the higher concentration of radiolysis products of water and air in Experiment B than Experiment A. Although no water was deliberately added to the vials used in Experiment B, there would have been some adsorbed $H_2O$ on the $UO_2$ surfaces [6] and on the glass walls at room temperature, in addition to the water present in the ambient air. It is well known that the radical oxidants formed during radiolysis of water (e.g., OH and $O_2^-$) can strongly enhance the oxidation of $UO_2$ [41]. The oxidation rates of $UO_2$ by the radical oxidants are several orders of magnitude higher than that by molecular $O_2$ [42].

Radiolysis of air leads to the formation of nitrogen oxides, $NO_x$, which can also participate in $UO_2$ oxidation [43]. The $NO_x$ formed in open system (Experiment A) can diffuse out, in addition to reacting with the $UO_2$ surface. In a closed system, however, $NO_x$ cannot diffuse out and hence is available for reaction with $UO_2$. This may also have contributed to the higher oxidation observed in Experiment B compared with Experiment A (Tables 1 and 3).

Our suggestion that the main reason for the higher oxidation observed in Experiment B compared with Experiment A is the higher concentrations of water and air radiolysis products is supported by the work of Campbell et al. [43] and Einziger et al. [44], who reported increased oxidation of $UO_2$ and PWR fuel in the presence of moisture (with gamma fields) and nitrogen oxides. On the other hand, $H_2O$ radiolysis products in the absence of $O_2$, Experiment D (Ar + 60% ss), do not seem to cause any oxidation of $UO_2$ at 150°C. The radiolysis of water produces both oxidants and reductants, e.g.,

$$H_2O \rightarrow OH + H \qquad (2)$$

(the OH radical is a potential oxidant, while H is a reductant). At room temperature, the radiolysis of water has been shown to cause $UO_2$ oxidation, even in the absence of $O_2$. For example, $UO_2$ oxidation has been observed in Ar-purged solutions undergoing radiolysis [41] due to the relatively higher reactivity of oxidants compared to that of reductants at room temperature. At higher temperatures, i.e., ~150°C, the increased reactivity of the reductants

cancels out any potential oxidation by the oxidants formed during radiolysis (the reactivity of $H_2$ is much higher at 150°C than at room temperature [15,45]).

The $UO_2$ samples in Experiment C ($O_2$ + 60% ss) appear to have undergone the most extensive oxidation. Surfaces of these samples are covered with $UO_3 \cdot xH_2O$ phases in addition to $U_3O_8$ phase(s), as discussed earlier (Sections 3.3 and 3.4). Taylor et al. observed the formation of similar $UO_3 \cdot xH_2O$ and $U_3O_8$ phases at ~225°C during air oxidation of unirradiated $UO_2$ under high humidity conditions [11,12,14]. They attributed the formation of these phases to the surface crystallization of $UO_2$ oxidation products in a "liquid-like" adsorbed water layer on $UO_2$. Also, XPS studies have shown that a surface layer with a $U^{6+}/U^{4+}$ ratio of ~2, i.e., that expected for $U_3O_8$, is formed on $UO_2$ electrodes at room temperature during potentiostatic oxidation of $UO_2$ at higher potentials [22]. Experiments have been started, under varying humidity conditions, to delineate the relative roles of radiolysis and the adsorbed water layer in the formation of $U_3O_8$ and $UO_3 \cdot xH_2O$ during oxidation of $UO_2$ at ~150°C.

Campbell et al. [43] have suggested that the radiolysis products of $N_2$ in air (e.g., $NO_2$) can increase the oxidation rate of $UO_2$. The increased oxidation in Experiment C ($O_2$ + 60% ss), which contained no $N_2$, compared with that in Experiments A and B, which contained both $N_2$ and $O_2$, suggests that the radiolysis products of $H_2O$ are probably much more significant than the radiolysis products of $N_2$ in terms of $UO_2$ oxidation. Further Experiments are planned to resolve the role of nitrogen oxides in $UO_2$ oxidation.

The results presented above show that $U_3O_8$ and higher oxides can form during $UO_2$ oxidation by air at 150°C in gamma fields similar to those associated with 10- to 20-year-old used CANDU fuel. The observation of traces of $U_3O_8$ in the most recent examination of CEX-1 fuel is consistent with this conclusion. Garisto [7] and, more recently, Kolar [46] have modelled the first stage in the oxidation of used fuel, i.e.,

$$3UO_2 + \tfrac{1}{2}O_2 \rightarrow U_3O_7 \qquad (3)$$

The results presented here suggest that the Reaction

$$3UO_2 + O_2 \rightarrow U_3O_8 \qquad (4)$$

can occur at 150°C in measurable amounts in the presence of gamma radiation.

Also, the Reaction

$$UO_2 + \tfrac{1}{2}O_2 \rightarrow UO_3 \qquad (5)$$

can occur at 150°C in the presence of gamma radiation if both $O_2$ and $H_2O$ are present. Therefore, we believe that any attempt to model the oxidation of used $UO_2$ fuel at 150°C by air and moist air should include Reactions (4) and (5).

The results presented here and those discussed by Campbell et al. [43] suggest that gamma radiolysis accelerates the oxidation of $UO_2$ by air and moist air. The gamma fields near the surface of a used fuel sample are a function not only of its burnup and cooling time but also of the amount of used fuel in the sample (and sample geometry). Thus, the dose rate near the surface of a used nuclear fuel sample consisting of a few grams will be much smaller than that near the surface of a fuel sample consisting of several kilograms (e.g., a complete fuel bundle). Therefore, we believe that the results of the laboratory Experiments, carried out using small fuel samples (i.e., a few grams), would underestimate the effects of gamma radiolysis on $UO_2$ oxidation for situations involving larger samples (e.g., several fuel bundles) unless external gamma fields are applied.

Although we are able to detect the formation of $U_3O_8$ on $UO_2$ samples exposed to air and gamma radiation at 150°C, the rate of growth of $U_3O_8$ in the absence of moisture (Experiment A) is quite slow. Thus, according to the calculated values in Table 3, the fraction of $U_3O_8$ present in the surface layer probed by XRD analysis is less than 0.7%. This represents a very slow rate of $UO_2$ oxidation to $U_3O_8$.

## 4. SUMMARY AND CONCLUSIONS

Oxidation of $UO_2$ at 150°C by air or $O_2$ in the presence of gamma fields equivalent to those associated with 10- to 20-year-old used CANDU fuel can lead to the formation of $U_3O_8$ on a $UO_2$ surface. The rate of formation of $U_3O_8$ on $UO_2$ in dry air at 150°C and gamma fields of ~15 Gy/h is very low. Oxidation of $UO_2$ to $U_3O_8$ (and $UO_3 \cdot xH_2O$) by air or $O_2$ in the presence of gamma radiation is strongly enhanced by the presence of water vapour. However, water vapour radiolysis, in the absence of $O_2$ (or other oxidizing agents), does not cause $UO_2$ oxidation at 150°C.

## ACKNOWLEDGEMENTS

We thank P. Taylor, R. McEachern, and K.M. Wasywich for helpful discussions and critical comments on the manuscript. The technical assistance of D.C. Doern (XRD data) and L.C. Brown (SEM micrographs) is acknowledged.

This work is part of the Canadian Nuclear Fuel Waste Management Program, which is jointly funded by AECL and Ontario Hydro under the auspices of the CANDU Owners Group.

REFERENCES


1. D.G. Boase and T.T. Vandergraaf. 1977. The Canadian Spent Fuel Storage Canister: Some Materials Aspects, Nucl. Technol. 32, 60.

2. I.E. Oldaker. 1979. The WNRE Program to Investigate the Stability of Irradiated CANDU Power-Reactor Fuel under Dry Storage Conditions, Atomic Energy of Canada Limited Report, AECL-6431.

3. K.M. Wasywich, J.D. Chen, C.R. Frost and J. Freire-Canosa. 1984. Long-Term Behaviour of Irradiated CANDU Fuel in Concrete Canister Storage - Test Results. In Irradiated Fuel Storage: Operating Experience and Development Programs, Toronto, Ontario, 1984, 393.

4. K.M. Wasywich and C.R. Frost. 1988. Canadian Experience with the Dry Storage of Used CANDU Fuel. In the Proceedings of the CNA Annual Conference at Winnipeg, Manitoba, June 12-15.

5. K.M. Wasywich, W.H. Hocking, D.W. Shoesmith and P. Taylor. 1993. Differences in Oxidation Behaviour of Used CANDU Fuel During Prolonged Storage in Moisture-Saturated Air and Dry Air at 150°C. Nucl. Tech. 104, 309.

6. P. Taylor, D.D. Wood, A.M. Duclos and D.G. Owen. 1989. Formation of Uranium Trioxide Hydrates on $UO_2$ Fuel in Air-Steam Mixtures Near 200°C. J. Nucl. Mater. 168, 70.

7. F. Garisto. 1993. Modelling the Oxidation of Defected Fuel Elements. Atomic Energy of Canada Limited Report, AECL-10734, COG-92-311.

8. H.J. Smith, J.C. Tait and R.E. Von Massow. 1987. Radioactive Decay Properties of Bruce "A" CANDU™ $UO_2$ Fuel and Recycle Waste. Atomic Energy of Canada Limited Report, AECL-9072.

9. W.H. Hocking, A.M. Duclos and L.H. Johnson. 1994. Study of Fission Product Segregation in Used CANDU Fuel by X-ray Photoelectron Spectroscopy (XPS) II. J. Nucl. Mater. 209, 1.

10. P. Taylor, E.A. Burgess and D.G. Owen. 1980. An X-ray Diffraction Study of the Formation of $\beta$-$UO_{2.33}$ on $UO_2$ Pellet Surfaces in Air at 229 to 275°C. J. Nucl. Mater. 88, 153.

11. P. Taylor, D.D. Wood, D.G. Owen and G.-I. Park. 1991. Crystallization of $U_3O_8$ and Hydrated $UO_3$ on $UO_2$ Fuel in Aerated Water near 200°C. J. Nucl. Mater. 183, 105.

12. P. Taylor, D.D. Wood, D.G. Owen, W.G. Hutchings and A.M. Duclos. 1991. Microstructures and Phase Relationships of Crystalline Oxidation Products Formed on Unused CANDU Fuel Exposed to Aerated Steam and Aerated Water near 200°C. Atomic Energy of Canada Limited Report, AECL-10476.

13. P. Taylor, D.D. Wood and A.M. Duclos. 1992. The Early Stages of $U_3O_8$ Formation on Fresh CANDU Fuel Oxidized in Air at 200-300°C. J. Nucl. Mater. 189, 116.

14. P. Taylor, R.L. Lemire and D.W. Wood. 1993 The Influence of Moisture on Air Oxidation of $UO_2$: Calculations and Observations. Nucl. Technol. 104, 164.

15. S. Sunder, G.D. Boyer and N.H. Miller. 1990. XPS Studies of $UO_2$ Oxidation by Alpha Radiolysis of Water at 100°C. J. Nucl. Mater. 175, 163.

16. Cullen, M.G. 1981. CEGB Steam Tables (Revised). Central Electricity Generating Board, London, U.K. Report # CC/N865, pp. 1-18.

17. M.A. Ryz. 1983. The Whiteshell Nuclear Research Establishment Immobilized Test Facility. Proceedings of the 31st Conference on Remote Systems Technology, Publ. Am. Nucl. Soc. pp 140-148.

18. S. Sunder, N.H. Miller and A.M. Duclos. 1994. XPS and XRD Studies of Samples from the Natural Fission Reactors in the Oklo Uranium Deposits. Mater. Res. Soc. Symp. Proc. 333 (Scientific Basis for Nuclear Waste Management XVII), pp. 631-8.

19. C.D. Wagner, W.M. Riggs, L.E. Davis, J.F. Moulder and G.E. Muilenberg. 1979. Handbook of X-ray Photoelectron Spectroscopy, Perkin-Elmer, Eden Prairie, Minnesota.

20. N.S. McIntyre, S. Sunder, D.W. Shoesmith and F.W. Stanchell. 1981. Chemical Information from XPS - Applications to the Analysis of Electrode Surfaces. J. Vac. Sci. Technol. 18, 714.

21. D. Briggs and M.P. Seah, Eds. 1983. Practical Surface Analysis by Auger and X-Ray Photoelectron Spectroscopy, J. Wiley & Sons, Chichester.

22. S. Sunder, D.W. Shoesmith, M.G. Bailey, F.W. Stanchell and N.S. McIntyre. 1981. Anodic Oxidation of $UO_2$. Part I, Electrochemical and X-ray Photoelectron Spectroscopic Studies in Neutral Solutions. J. Electroanal. Chem. 130, 163.

23. J. Verbist, J. Riga, C. Tenret-Noel, J.J. Pireaux, G. d'Ursel, R. Caudano and E.G. Derouane. 1976. Bonding and Valence in Uranium Compounds with Oxygen: A Study by X-ray Photoelectron Spectroscopy and Electron Paramagnetic Resonance. In Plutonium and other Actinides, eds. H. Blank and R. Lindner. North-Holland, Amsterdam, pp. 409-419.

24. B.W. Veal and D.J. Lam. 1982. Photoemission Spectra in Gmelin Handbook of Inorganic Chemistry Suppl. Vol. A5. Springer Verlag, Heidelberg pp. 176-196.

25. G.C. Allan, P.A. Tempest and J.W. Tyler. 1987. J. Chem. Soc. Faraday Trans. I., 83, 925.

26. G.C. Allen and N.R. Holmes. 1987. Surface Characterisation of α-, β-, γ-, and δ-$UO_3$ Using X-Ray Photoelectron Spectroscopy. J. Chem. Soc. Dalton Trans., 3009.

27. G.C. Allen, P.A. Tempest and J.W. Tyler. 1987. Oxidation of Crystalline $UO_2$ Studied Using X-ray Photoelectron Spectroscopy and X-ray Diffraction. J. Chem. Soc. Faraday Trans. 1, 83, 925.

28. S. Sunder, J.J. Cramer and N.H. Miller. 1992. X-ray Photoelectron Spectroscopic Study of Cigar Lake Uranium Ore: A Natural Analog for Used Fuel. Mater. Res. Soc. Symp. Proc. 257, Scientific Basis for Nuclear Waste Management, XV, pp. 449-457.

29. H.R. Hoekstra, A. Santoro and S. Siegel. 1961. The Low Temperature Oxidation of $UO_2$ and $U_4O_9$. J. Inorg. Nucl. Chem. 18 166.

30. D.K. Smith, B.E. Scheetz, C.A.F. Anderson and K.L. Smith. 1982. Phase Relations in the Uranium-Oxygen-Water System and Its Significance on the Stability of Nuclear Waste Forms. Uranium, 1, 79.

31. D. Vollath. 1984. In Uranium-Uranium Dioxide, $UO_2$, Preparation and Crystallographic Properties. Gmelin Handbook of Inorganic Chemistry, Vol. C4, Springer-Verlag, Heidelberg, p. 97.

32. J. Janeczek, and R.C. Ewing. 1991. X-ray Powder Diffraction Study of Annealed Uraninite. J. Nucl. Mater. 185, 66.

33. L.E. Thomas, R.E. Einziger and H.C. Buchanan. 1993. Effect of Fission Products on Air-Oxidation of LWR Spent Fuel. J. Nucl. Mater. 201, 310.

34. B.T. Willis. 1987. Crystallographic Studies of Anion-excess Uranium Oxides. J. Chem. Soc. 83, 1073-1081.

35. P.A. Tempest, P.N. Tucker and J.W. Tyler, 1988. Oxidation of $UO_2$ Fuel Pellets in Air at 503 and 543 K Studied Using X-ray Photoelectron Spectroscopy and X-ray Diffraction. J. Nucl. Mater. 185, 251.

36. Powder Diffraction Files. 1994. Inorganic Materials, Inter. Center for Diffraction Data, Newtown Square, Penn.

37. J.W. Choi, R. McEachern and P. Taylor, unpublished work.

38. P. Taylor, Unpublished work.

39. P.M. Tucker. 1987. The Effect of Oxygen Partial Pressure on the Kinetics of Unirradiated $UO_2$ Oxidation. In Chemical Reactivity of Oxide Fuel and Fission Product Release. Vol. 1, K.A. Simpson and P. Wood (eds.), Central Electricity Generating Board, London, U.K.

40. J. Nakamura, T. Otomo and S. Kawasaki. 1993. Oxidation of $UO_2$ Under Dry Storage Conditions. J. Nucl. Sc. Tech. 30, 181.

41. S. Sunder, D.W. Shoesmith, H. Christensen, N.H. Miller and M.G. Bailey. 1990. Oxidation of $UO_2$ Fuel by Radicals Formed During Radiolysis of Water. Mater. Res. Soc. Symp. Proc., 176, (Scientific Basis for Nuclear Waste Management XIII), pp. 457-464.

42. H. Christensen, S. Sunder and D.W. Shoesmith. 1994. Oxidation of Nuclear Fuel $UO_2$ by the Products of Water Radiolysis Development of a Kinetic Model. J. Alloys and Compounds. 213/214, 93.

43. T.K. Campbell, E.R. Gilbert, G.D. White, G.F. Piepel and B.J. Wrona. 1989. Oxidation Behaviour of Nonirradiated $UO_2$. Nucl. Technol. 85, 160.

44. R.E. Einziger, S.C. Marschman and H.C. Buchanan. 1991. Spent Fuel Dry-Bath Oxidation Testing. Nucl. Technol. 94, 383.

45. G.V. Buxton, C.L. Greenstock, W.P. Helmand and A.B. Ross. 1988. Critical Review of Rate Constants for Reactions of Hydrated Electrons, Hydrogen Atoms and Hydroxyl Radicals in Aqueous Solution. J. Phys. Chem. Ref. Data, 17, 513.

46. M. Kolar. 1994. Application of the Integral Method to Modelling the Oxidation of Defected Fuel Elements. Atomic Energy of Canada Limited Report, AECL-11174, COG-1-94-446.

---

* Unrestricted, unpublished report available from Scientific Document Distribution Office, Chalk River Laboratories, Chalk River, Ontario, Canada KOJ 1J0.

# APPENDIX A

## DOSE RATE IN THE EXPERIMENT

## APPENDIX A

## DOSE RATE IN THE EXPERIMENT

The used fuel samples surrounding the Experiments described here were part of the Experiment called ACX-1, alternate controlled environment Experiment, also called CEX-2 (Sections 1 and 2.1 of main text). To estimate gamma dose rate experienced by the $UO_2$ samples used in present study the dose rate measurements were carried out at the beginning of the Experiment ACX-2 as the gamma dose rate during these Experiments (and ACX-1) was not measured. ACX-2 uses the same Experimental set-up, but contains one less fuel rod in each of the four fuel vessels, Figure 3. (These fuel rods were removed for examination). Thus, the total number of fuel rods in the ACX-2 Experiment is 48 instead of 52 in the ACX-1. The dose rate was measured, using a Curie Pie Model CPMU # 01743 obtained from Technical Associate Canoga Park, CA. U.S.A., at two points: (a) at the top of the aluminum vessel (T in Figure A-1), $R_T$ = 3.20 Gy/h; and (b) and at a point 15 cm above the top of the aluminum-vessel (T' in Figure A-1), $R_{T'}$ = 1.40 Gy/h. Here $R_T$ and $R_{T'}$ are measured dose rates at points T and T'.

In order to calculate gamma dose rate experienced by the $UO_2$ samples from the above measured values, we approximate the used fuel rods surrounding the aluminum vessel with a point source located at a distance equal to the distance between the centre axes of the fuel vessels and of the aluminum sample vessel (A and B, respectively, in Figures 3 and A-1); and at a height equal to the middle of the aluminum vessel (A in Figure A-1). With these approximations the dose rate at the centre of the aluminum vessel (B in Figure A-1), $R_B$ is:

$$\begin{aligned} R_B &= R_T \cdot (AT^2/AB^2) \\ &= R_T \cdot [(AB^2+BT^2)/AB^2] \\ &= 3.20 \cdot [(15.6^2 + 31^2)/15.6^2] \text{ Gy/h} \\ &\sim 15 \text{ Gy/h} \ . \end{aligned}$$

Here AB and BT are 15.6 and 31 cm, respectively.

If we use the same procedure to calculate the dose rate at T' from the measured value at T (TT' = 15 cm), i.e.:

$$\begin{aligned} R_{T'} &= R_T \cdot (AT^2/AT'^2) \\ &= R_T \cdot (AT^2/(AB + TT')^2) \\ &= 3.20 \cdot ((15.6^2 + 31^2)/ (15.6^2 + (31 + 15.0)^2)) \text{ Gy/h} \\ &\sim 1.6 \text{ Gy/h} \ . \end{aligned}$$

This compares favourably with the measured value of $R_{T'}$, i.e., 1.4 Gy/h and gives confidence in the assumptions made in the above calculations. Thus, the dose rate in the aluminum vessel varies along the vertical axis between 15 and 3.4 Gy/h. These dose rate are similar to those expected on the surface of 10 to 20 a old CANDU fuel [A1]. The dose rate in the

aluminum vessel would decrease with an increase in the distance from the middle point. However, the dose rate would increase with an increase in the distance from the centre of the aluminum vessel, i.e., the points closer to the used fuel (away from the centre axis of aluminum vessel) would experience higher gamma fields. We believe that the dose rate experienced by the $UO_2$ samples was closer to 15 Gy/h during the Experiment as the samples were closer to the middle of the aluminum vessel.

## REFERENCE

A.1 D.W. Shoesmith and S. Sunder. 1992. The Prediction of Nuclear Fuel ($UO_2$) Dissolution Rates Under Waste Disposal Conditions. J. Nucl. Mater. 190, 20.

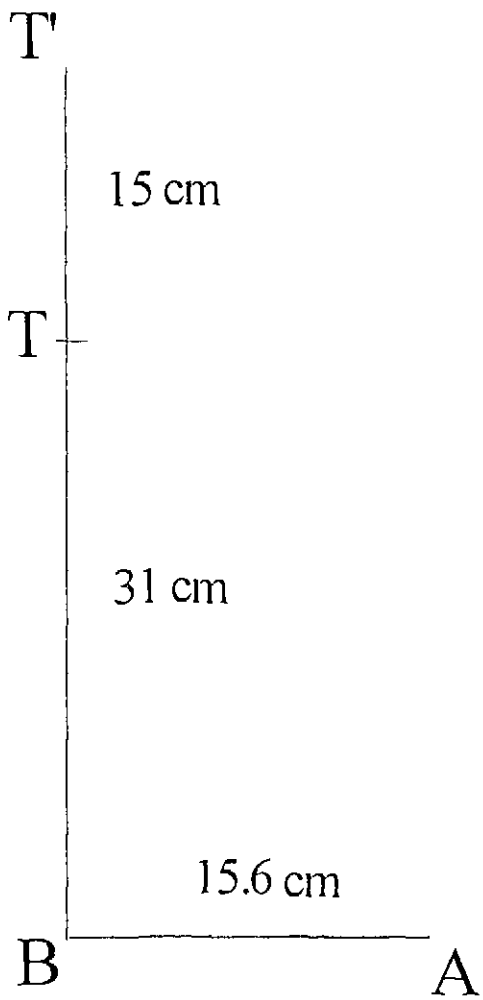


*FIGURE A-1:* Schematic of Locations Used for Calculating Dose Rate: A, Centre of Fuel Vessel; B, Centre of Aluminum Vessel Containing $UO_2$ Samples (see Figure 3); and T, Top of the Aluminum Vessel. T and T' are Locations of Dose Rate Measurements (see text).

# APPENDIX B

# APPENDIX B

## TABLE B-1

## XRD DATA FOR $UO_2$ OXIDATION AT 150°C IN GAMMA RADIATION IN OPEN AIR

(Sample M, Experiment A)

| | Peak-Position | | Centroid-Position | | Peak & Area are without Bkgrd* | | | | | |
|---|---|---|---|---|---|---|---|---|---|---|
| # | 2Theta | d | 2Theta | d | Bkgrd | Peak | I% | Area | I% | FWHM |
| 1: | 21.470 | 4.1355 | 21.467 | 4.1360 | 90 | 3922 | 26.9 | 892 | 8.6 | 0.205 |
| 2: | 26.150 | 3.4050 | 26.140 | 3.4062 | 141 | 112 | 0.8 | 56 | 0.5 | 0.450 |
| 3: | 28.170 | 3.1652 | 28.170 | 3.1652 | 146 | 8008 | 54.9 | 3751 | 36.3 | 0.422 |
| 4: | 28.510 | 3.1283 | 28.511 | 3.1281 | 140 | 14587 | 100.0 | 10326 | 100.0 | 0.637 |
| 5: | 28.770 | 3.1006 | 28.755 | 3.1022 | 132 | 13231 | 90.7 | 3899 | 37.8 | 0.265 |
| 6: | 32.690 | 2.7372 | 32.691 | 2.7371 | 93 | 3238 | 22.2 | 2226 | 21.6 | 0.619 |
| 7: | 33.260 | 2.6916 | 33.260 | 2.6915 | 81 | 6542 | 44.8 | 3348 | 32.4 | 0.461 |
| 8: | 33.560 | 2.6682 | 33.560 | 2.6682 | 88 | 2424 | 16.6 | 980 | 9.5 | 0.364 |
| 9: | 36.521 | 2.4584 | 36.528 | 2.4579 | 51 | 76 | 0.5 | 17 | 0.2 | 0.201 |
| 10: | 40.340 | 2.2340 | 40.338 | 2.2341 | 54 | 55 | 0.4 | 23 | 0.2 | 0.376 |
| 11: | 43.680 | 2.0706 | 43.690 | 2.0702 | 73 | 503 | 3.4 | 175 | 1.7 | 0.313 |
| 12: | 46.680 | 1.9443 | 46.690 | 1.9439 | 108 | 2219 | 15.2 | 1200 | 11.6 | 0.487 |
| 13: | 46.990 | 1.9322 | 46.999 | 1.9318 | 101 | 4361 | 29.9 | 3885 | 37.6 | 0.802 |
| 14: | 47.380 | 1.9172 | 47.382 | 1.9171 | 101 | 3294 | 22.6 | 5043 | 48.8 | 1.378 |
| 15: | 47.880 | 1.8983 | 47.873 | 1.8986 | 120 | 4520 | 31.0 | 3271 | 31.7 | 0.651 |
| 16: | 51.600 | 1.7699 | 51.597 | 1.7700 | 85 | 237 | 1.6 | 217 | 2.1 | 0.824 |
| 17: | 55.740 | 1.6478 | 55.746 | 1.6476 | 250 | 3869 | 26.5 | 2420 | 23.4 | 0.563 |
| 18: | 55.909 | 1.6432 | 55.906 | 1.6433 | 243 | 2515 | 17.2 | 2647 | 25.6 | 0.947 |
| 19: | 56.560 | 1.6259 | 56.559 | 1.6259 | 329 | 4519 | 31.0 | 2885 | 27.9 | 0.575 |
| 20: | 57.391 | 1.6043 | 57.405 | 1.6039 | 671 | 304 | 2.1 | 75 | 0.7 | 0.222 |
| 21: | 58.440 | 1.5779 | 58.452 | 1.5777 | 309 | 840 | 5.8 | 204 | 2.0 | 0.219 |
| 22: | 59.040 | 1.5633 | 59.037 | 1.5634 | 258 | 711 | 4.9 | 839 | 8.1 | 0.062 |
| 23: | 59.510 | 1.5521 | 59.506 | 1.5522 | 211 | 658 | 4.5 | 415 | 4.0 | 0.568 |
| 24: | 67.840 | 1.3804 | 67.838 | 1.3804 | 124 | 132 | 0.9 | 77 | 0.7 | 0.525 |
| 25: | 68.600 | 1.3669 | 68.605 | 1.3668 | 152 | 582 | 4.0 | 139 | 1.3 | 0.215 |
| 26: | 68.800 | 1.3634 | 68.797 | 1.3635 | 106 | 315 | 2.2 | 319 | 3.1 | 0.911 |
| 27: | 69.770 | 1.3468 | 69.771 | 1.3468 | 143 | 590 | 4.0 | 274 | 2.7 | 0.418 |
| 28: | 70.380 | 1.3367 | 70.389 | 1.3365 | 129 | 114 | 0.8 | 55 | 0.5 | 0.434 |
| 29: | 75.780 | 1.2543 | 75.782 | 1.2542 | 421 | 1795 | 12.3 | 399 | 3.9 | 0.200 |
| 30: | 76.000 | 1.2512 | 75.998 | 1.2512 | 362 | 1081 | 7.4 | 891 | 8.6 | 0.742 |
| 31: | 76.580 | 1.2431 | 76.581 | 1.2431 | 321 | 618 | 4.2 | 1435 | 13.9 | 2.090 |

continued...

TABLE B-1 (concluded)

| | Peak-Position | | Centroid-Position | | Peak & Area are without Bkgrd* | | | | | |
|---|---|---|---|---|---|---|---|---|---|---|
| # | 2Theta | d | 2Theta | d | Bkgrd | Peak | I% | Area | I% | FWHM |
| 32: | 76.740 | 1.2409 | 76.742 | 1.2409 | 346 | 631 | 4.3 | 1372 | 13.3 | 1.957 |
| 33: | 77.070 | 1.2364 | 77.069 | 1.2365 | 408 | 602 | 4.1 | 1155 | 11.2 | 1.727 |
| 34: | 77.550 | 1.2300 | 77.542 | 1.2301 | 445 | 531 | 3.6 | 787 | 7.6 | 1.334 |
| 35: | 78.110 | 1.2226 | 78.112 | 1.2225 | 557 | 1048 | 7.2 | 148 | 1.4 | 0.127 |
| 36: | 78.340 | 1.2196 | 78.334 | 1.2196 | 526 | 418 | 2.9 | 50 | 0.5 | 0.108 |
| 37: | 79.360 | 1.2064 | 79.361 | 1.2064 | 327 | 627 | 4.3 | 465 | 4.5 | 0.667 |
| 38: | 79.580 | 1.2036 | 79.564 | 1.2038 | 307 | 487 | 3.3 | 483 | 4.7 | 0.893 |
| 39: | 80.470 | 1.1925 | 80.470 | 1.1925 | 255 | 17 | 0.1 | 1 | 0.0 | 0.053 |
| 40: | 87.280 | 1.1162 | 87.285 | 1.1161 | 225 | 1652 | 11.3 | 438 | 4.2 | 0.239 |
| 41: | 87.550 | 1.1134 | 87.548 | 1.1134 | 194 | 830 | 5.7 | 890 | 8.6 | 0.965 |
| 42: | 88.280 | 1.1061 | 88.291 | 1.1060 | 190 | 446 | 3.1 | 783 | 7.6 | 1.580 |
| 43: | 88.530 | 1.1036 | 88.532 | 1.1036 | 191 | 595 | 4.1 | 674 | 6.5 | 1.019 |
| 44: | 88.710 | 1.1018 | 88.707 | 1.1019 | 190 | 568 | 3.9 | 622 | 6.0 | 0.986 |
| 45: | 90.000 | 1.0894 | 90.003 | 1.0893 | 193 | 33 | 0.2 | 4 | 0.0 | 0.109 |
| 46: | 94.100 | 1.0524 | 94.102 | 1.0524 | 251 | 1480 | 10.1 | 323 | 3.1 | 0.196 |
| 47: | 94.410 | 1.0498 | 94.405 | 1.0498 | 269 | 657 | 4.5 | 122 | 1.2 | 0.167 |
| 48: | 95.890 | 1.0374 | 95.891 | 1.0374 | 231 | 597 | 4.1 | 500 | 4.8 | 0.754 |
| 49: | 105.640 | 0.9668 | 105.647 | 0.9668 | 135 | 598 | 4.1 | 148 | 1.4 | 0.223 |
| 50: | 106.030 | 0.9643 | 106.025 | 0.9644 | 146 | 265 | 1.8 | 101 | 1.0 | 0.343 |
| 51: | 108.220 | 0.9508 | 108.226 | 0.9508 | 151 | 93 | 0.6 | 69 | 0.7 | 0.668 |
| 52: | 112.870 | 0.9244 | 112.874 | 0.9244 | 327 | 1945 | 13.3 | 452 | 4.4 | 0.209 |
| 53: | 113.310 | 0.9221 | 113.306 | 0.9221 | 362 | 831 | 5.7 | 216 | 2.1 | 0.234 |
| 54: | 115.360 | 0.9115 | 115.360 | 0.9115 | 411 | 1476 | 10.1 | 704 | 6.8 | 0.429 |
| 55: | 115.800 | 0.9093 | 115.799 | 0.9093 | 403 | 659 | 4.5 | 282 | 2.7 | 0.385 |

* Intensity values are based on counts per second.

TABLE B-2

XRD DATA FOR $UO_2$ OXIDATION AT 150°C IN GAMMA RADIATION IN CLOSED AIR

(Sample L, Experiment B)

| | Peak-Position | | Centroid-Position | | | Peak & Area are without Bkgrd* | | | | |
|---|---|---|---|---|---|---|---|---|---|---|
| # | 2Theta | d | 2Theta | d | Bkgrd | Peak | I% | Area | I% | FWHM |
| 1: | 21.440 | 4.1412 | 21.436 | 4.1420 | 129 | 13484 | 100.0 | 3062 | 45.3 | 0.204 |
| 2: | 25.220 | 3.5284 | 25.219 | 3.5285 | 161 | 436 | 3.2 | 224 | 3.3 | 0.462 |
| 3: | 25.960 | 3.4295 | 25.963 | 3.4291 | 191 | 868 | 6.4 | 608 | 9.0 | 0.630 |
| 4: | 28.040 | 3.1796 | 28.044 | 3.1792 | 201 | 6550 | 48.6 | 3336 | 49.3 | 0.458 |
| 5: | 28.460 | 3.1337 | 28.456 | 3.1341 | 190 | 8149 | 60.4 | 6762 | 100.0 | 0.747 |
| 6: | 32.360 | 2.7643 | 32.365 | 2.7640 | 346 | 3530 | 26.2 | 1939 | 28.7 | 0.494 |
| 7: | 33.210 | 2.6955 | 33.211 | 2.6954 | 118 | 4140 | 30.7 | 3911 | 57.8 | 0.850 |
| 8: | 33.750 | 2.6536 | 33.748 | 2.6538 | 155 | 1545 | 11.5 | 1656 | 24.5 | 0.965 |
| 9: | 43.650 | 2.0720 | 43.656 | 2.0717 | 95 | 2032 | 15.1 | 627 | 9.3 | 0.278 |
| 10 | 46.550 | 1.9494 | 46.550 | 1.9494 | 134 | 2369 | 17.6 | 2016 | 29.8 | 0.766 |
| 11 | 46.960 | 1.9333 | 46.964 | 1.9332 | 155 | 2887 | 21.4 | 4076 | 60.3 | 1.271 |
| 12 | 47.690 | 1.9054 | 47.689 | 1.9055 | 193 | 2047 | 15.2 | 2036 | 30.1 | 0.895 |
| 13 | 51.470 | 1.7740 | 51.468 | 1.7741 | 136 | 1331 | 9.9 | 1427 | 21.1 | 0.965 |
| 14 | 54.779 | 1.6744 | 54.768 | 1.6747 | 1007 | 298 | 2.2 | 91 | 1.3 | 0.275 |
| 15 | 55.420 | 1.6566 | 55.423 | 1.6565 | 306 | 1136 | 8.4 | 1957 | 28.9 | 1.550 |
| 16 | 55.700 | 1.6489 | 55.703 | 1.6488 | 328 | 2287 | 17.0 | 2630 | 38.9 | 1.035 |
| 17 | 55.870 | 1.6443 | 55.865 | 1.6444 | 337 | 1515 | 11.2 | 2299 | 34.0 | 1.366 |
| 18 | 56.510 | 1.6272 | 56.509 | 1.6272 | 563 | 2351 | 17.4 | 1222 | 18.1 | 0.468 |
| 19 | 58.410 | 1.5787 | 58.419 | 1.5785 | 311 | 525 | 3.9 | 542 | 8.0 | 0.929 |
| 20 | 58.980 | 1.5648 | 58.981 | 1.5648 | 250 | 428 | 3.2 | 357 | 5.3 | 0.751 |
| 21 | 64.650 | 1.4406 | 64.652 | 1.4405 | 74 | 188 | 1.4 | 299 | 4.4 | 1.431 |
| 22 | 67.770 | 1.3816 | 67.770 | 1.3816 | 113 | 457 | 3.4 | 315 | 4.7 | 0.620 |
| 23 | 68.580 | 1.3673 | 68.573 | 1.3674 | 136 | 371 | 2.8 | 125 | 1.8 | 0.303 |
| 24 | 69.710 | 1.3479 | 69.708 | 1.3479 | 147 | 441 | 3.3 | 197 | 2.9 | 0.402 |
| 25 | 73.800 | 1.2829 | 73.802 | 1.2829 | 286 | 230 | 1.7 | 168 | 2.5 | 0.657 |
| 26 | 74.760 | 1.2688 | 74.760 | 1.2688 | 384 | 140 | 1.0 | 105 | 1.6 | 0.675 |
| 27 | 75.740 | 1.2548 | 75.743 | 1.2548 | 452 | 953 | 7.1 | 189 | 2.8 | 0.178 |
| 28 | 75.970 | 1.2516 | 75.965 | 1.2517 | 451 | 526 | 3.9 | 258 | 3.8 | 0.441 |
| 29 | 76.510 | 1.2441 | 76.514 | 1.2440 | 415 | 410 | 3.0 | 666 | 9.8 | 1.462 |
| 30 | 76.780 | 1.2404 | 76.780 | 1.2404 | 407 | 445 | 3.3 | 594 | 8.8 | 1.201 |
| 31 | 78.070 | 1.2231 | 78.072 | 1.2231 | 439 | 638 | 4.7 | 100 | 1.5 | 0.141 |
| 32 | 78.300 | 1.2201 | 78.294 | 1.2201 | 408 | 254 | 1.9 | 32 | 0.5 | 0.113 |

continued ...

TABLE B-2 (concluded)

| | Peak-Position | | Centroid-Position | | | Peak & Area are without Bkgrd* | | | | |
|---|---|---|---|---|---|---|---|---|---|---|
| # | 2Theta | d | 2Theta | d | Bkgrd | Peak | I% | Area | I% | FWHM |
| 33 | 79.290 | 1.2073 | 79.293 | 1.2073 | 277 | 395 | 2.9 | 261 | 3.9 | 0.595 |
| 34 | 85.510 | 1.1347 | 85.510 | 1.1347 | 221 | 140 | 1.0 | 120 | 1.8 | 0.771 |
| 35 | 87.230 | 1.1167 | 87.237 | 1.1166 | 293 | 891 | 6.6 | 208 | 3.1 | 0.210 |
| 36 | 87.520 | 1.1137 | 87.509 | 1.1138 | 260 | 448 | 3.3 | 220 | 3.3 | 0.442 |
| 37 | 88.620 | 1.1027 | 88.620 | 1.1027 | 220 | 354 | 2.6 | 373 | 5.5 | 0.948 |
| 38 | 94.070 | 1.0527 | 94.065 | 1.0527 | 245 | 1010 | 7.5 | 235 | 3.5 | 0.209 |
| 39 | 94.360 | 1.0502 | 94.359 | 1.0502 | 247 | 412 | 3.1 | 84 | 1.2 | 0.183 |
| 40 | 95.790 | 1.0383 | 95.792 | 1.0382 | 199 | 435 | 3.2 | 343 | 5.1 | 0.710 |
| 41 | 101.880 | 0.9920 | 101.878 | 0.9920 | 98 | 154 | 1.1 | 177 | 2.6 | 1.034 |
| 42 | 105.600 | 0.9671 | 105.602 | 0.9671 | 163 | 413 | 3.1 | 98 | 1.4 | 0.214 |
| 43 | 105.990 | 0.9646 | 105.981 | 0.9646 | 173 | 168 | 1.2 | 42 | 0.6 | 0.225 |
| 44 | 112.850 | 0.9246 | 112.839 | 0.9246 | 379 | 1316 | 9.8 | 364 | 5.4 | 0.249 |
| 45 | 113.270 | 0.9223 | 113.261 | 0.9224 | 408 | 637 | 4.7 | 192 | 2.8 | 0.271 |
| 46 | 115.330 | 0.9117 | 115.323 | 0.9117 | 387 | 927 | 6.9 | 512 | 7.6 | 0.497 |
| 47 | 115.770 | 0.9095 | 115.763 | 0.9095 | 364 | 396 | 2.9 | 158 | 2.3 | 0.359 |

* Intensity values are based on counts per second.

TABLE B-3

XRD DATA FOR $UO_2$ OXIDATION AT 150°C IN GAMMA RADIATION

($O_2$ + 60% Saturated Steam; Sample X, Experiment C)

| | Peak-Position | | Centroid-Position | | | Peak & Area are without Bkgrd* | | | | |
|---|---|---|---|---|---|---|---|---|---|---|
| # | 2Theta | d | 2Theta | d | Bkgrd | Peak | I% | Area | I% | FWHM |
| 1: | 11.500 | 7.6885 | 11.499 | 7.6890 | 266 | 1852 | 15.2 | 598 | 26.4 | 0.291 |
| 2: | 13.540 | 6.5344 | 13.537 | 6.5360 | 295 | 1177 | 9.7 | 299 | 13.2 | 0.229 |
| 3: | 14.080 | 6.2849 | 14.079 | 6.2853 | 245 | 3754 | 30.8 | 1050 | 46.4 | 0.252 |
| 4: | 15.380 | 5.7564 | 15.385 | 5.7546 | 285 | 301 | 2.5 | 163 | 7.2 | 0.487 |
| 5: | 17.440 | 5.0809 | 17.430 | 5.0837 | 201 | 12194 | 100.0 | 2263 | 100.0 | 0.167 |
| 6: | 18.490 | 4.7947 | 18.487 | 4.7954 | 188 | 516 | 4.2 | 146 | 6.5 | 0.255 |
| 7: | 19.050 | 4.6550 | 19.046 | 4.6560 | 178 | 874 | 7.2 | 258 | 11.4 | 0.266 |
| 8: | 19.500 | 4.5486 | 19.494 | 4.5501 | 170 | 2356 | 19.3 | 561 | 24.8 | 0.214 |
| 9: | 21.430 | 4.1431 | 21.423 | 4.1444 | 135 | 1048 | 8.6 | 202 | 8.9 | 0.173 |
| 10: | 23.110 | 3.8456 | 23.113 | 3.8450 | 172 | 493 | 4.0 | 175 | 7.7 | 0.319 |
| 11: | 23.410 | 3.7970 | 23.389 | 3.8003 | 182 | 292 | 2.4 | 114 | 5.0 | 0.351 |
| 12: | 24.079 | 3.6930 | 24.076 | 3.6934 | 220 | 84 | 0.7 | 18 | 0.8 | 0.193 |
| 13: | 24.400 | 3.6451 | 24.392 | 3.6463 | 235 | 127 | 1.0 | 18 | 0.8 | 0.128 |
| 14: | 24.960 | 3.5646 | 24.961 | 3.5644 | 533 | 570 | 4.7 | 115 | 5.1 | 0.182 |
| 15: | 25.590 | 3.4782 | 25.606 | 3.4761 | 421 | 4252 | 34.9 | 1787 | 79.0 | 0.378 |
| 16: | 25.770 | 3 4544 | 25.770 | 3.4543 | 443 | 2930 | 24.0 | 1171 | 51.7 | 0.360 |
| 17: | 26.330 | 3.3821 | 26.332 | 3.3819 | 500 | 2206 | 18.1 | 823 | 36.4 | 0.336 |
| 18: | 26.670 | 3.3398 | 26.670 | 3.3398 | 556 | 5550 | 45.5 | 1523 | 67.3 | 0.247 |
| 19: | 27.420 | 3.2501 | 27.428 | 3.2491 | 599 | 796 | 6.5 | 269 | 11.9 | 0.304 |
| 20: | 28.100 | 3.1730 | 28.112 | 3.1716 | 491 | 1756 | 14.4 | 616 | 27.2 | 0.316 |
| 21: | 28.420 | 3.1380 | 28.419 | 3.1381 | 476 | 2308 | 18.9 | 1697 | 75.0 | 0.662 |
| 22: | 28.760 | 3.1016 | 28.753 | 3.1024 | 428 | 2818 | 23.1 | 856 | 37.8 | 0.273 |
| 23: | 29.180 | 3.0579 | 29.179 | 3.0580 | 444 | 718 | 5.9 | 239 | 10.6 | 0.300 |
| 24: | 29.930 | 2.9830 | 29.934 | 2.9826 | 283 | 516 | 4.2 | 143 | 6.3 | 0.249 |
| 25: | 31.130 | 2.8707 | 31.136 | 2.8701 | 262 | 2262 | 18.6 | 622 | 27.5 | 0.247 |
| 26: | 31.970 | 2.7972 | 31.968 | 2.7973 | 322 | 82 | 0.7 | 15 | 0.7 | 0.165 |
| 27: | 32.410 | 2.7601 | 32.430 | 2.7586 | 317 | 548 | 4.5 | 165 | 7.3 | 0.271 |
| 28: | 32.620 | 2.7429 | 32.618 | 2.7431 | 327 | 638 | 5.2 | 341 | 15.1 | 0.481 |
| 29: | 32.970 | 2.7146 | 32.978 | 2.7139 | 350 | 1049 | 8.6 | 814 | 36.0 | 0.698 |
| 30: | 33.190 | 2.6971 | 33.174 | 2.6984 | 359 | 878 | 7.2 | 607 | 26.8 | 0.622 |
| 31: | 33.510 | 2.6721 | 33.500 | 2.6728 | 371 | 493 | 4.0 | 128 | 5.7 | 0.234 |
| 32: | 33.980 | 2.6362 | 33.975 | 2.6366 | 378 | 131 | 1.1 | 34 | 1.5 | 0.234 |

continued...

TABLE B-3 (continued)

| | Peak-Position | | Centroid-Position | | | Peak & Area are without Bkgrd* | | | | |
|---|---|---|---|---|---|---|---|---|---|---|
| # | 2Theta | d | 2Theta | d | Bkgrd | Peak | I% | Area | I% | FWHM |
| 33: | 34.310 | 2.6116 | 34.304 | 2.6120 | 389 | 111 | 0.9 | 22 | 1.0 | 0.178 |
| 34: | 35.280 | 2.5419 | 35.285 | 2.5416 | 270 | 1982 | 16.3 | 705 | 31.2 | 0.320 |
| 35: | 36.040 | 2.4901 | 36.040 | 2.4901 | 245 | 1315 | 10.8 | 651 | 28.8 | 0.446 |
| 36: | 36.420 | 2.4650 | 36.414 | 2.4654 | 206 | 871 | 7.1 | 270 | 11.9 | 0.279 |
| 37: | 37.630 | 2.3884 | 37.619 | 2.3891 | 130 | 85 | 0.7 | 24 | 1.1 | 0.254 |
| 38: | 38.640 | 2.3283 | 38.641 | 2.3282 | 160 | 250 | 2.1 | 54 | 2.4 | 0.194 |
| 39: | 40.010 | 2.2517 | 40.012 | 2.2516 | 161 | 324 | 2.7 | 165 | 7.3 | 0.458 |
| 40: | 40.770 | 2.2114 | 40.768 | 2.2115 | 173 | 234 | 1.9 | 75 | 3.3 | 0.288 |
| 41: | 42.380 | 2.1311 | 42.392 | 2.1305 | 240 | 188 | 1.5 | 45 | 2.0 | 0.215 |
| 42: | 43.130 | 2.0957 | 43.126 | 2.0959 | 324 | 224 | 1.8 | 57 | 2.5 | 0.229 |
| 43: | 43.630 | 2.0729 | 43.640 | 2.0724 | 375 | 144 | 1.2 | 27 | 1.2 | 0.169 |
| 44: | 44.090 | 2.0523 | 44.102 | 2.0518 | 351 | 798 | 6.5 | 225 | 9.9 | 0.254 |
| 45: | 44.780 | 2.0223 | 44.782 | 2.0222 | 407 | 499 | 4.1 | 186 | 8.2 | 0.335 |
| 46: | 45.890 | 1.9759 | 45.889 | 1.9760 | 565 | 729 | 6.0 | 184 | 8.1 | 0.227 |
| 47: | 46.670 | 1.9447 | 46.674 | 1.9445 | 383 | 1036 | 8.5 | 1458 | 64.4 | 1.267 |
| 48: | 46.950 | 1.9337 | 46.952 | 1.9337 | 372 | 916 | 7.5 | 1779 | 78.6 | 1.748 |
| 49: | 47.900 | 1.8976 | 47.893 | 1.8978 | 459 | 1007 | 8.3 | 352 | 15.6 | 0.315 |
| 50: | 48.930 | 1.8600 | 48.943 | 1.8596 | 303 | 226 | 1.9 | 58 | 2.6 | 0.231 |
| 51: | 49.829 | 1.8285 | 49.828 | 1.8286 | 288 | 96 | 0.8 | 41 | 1.8 | 0.384 |
| 52: | 51.300 | 1.7795 | 51.306 | 1.7793 | 278 | 994 | 8.2 | 641 | 28.3 | 0.580 |
| 53: | 51.630 | 1.7689 | 51.629 | 1.7689 | 278 | 827 | 6.8 | 601 | 26.6 | 0.654 |
| 54: | 52.800 | 1.7324 | 52.797 | 1.7325 | 299 | 507 | 4.2 | 239 | 10.6 | 0.424 |
| 55: | 54.080 | 1.6944 | 54.080 | 1.6944 | 353 | 610 | 5.0 | 181 | 8.0 | 0.267 |
| 56: | 54.930 | 1.6702 | 54.931 | 1.6701 | 423 | 500 | 4.1 | 254 | 11.2 | 0.457 |
| 57: | 55.460 | 1.6555 | 55.473 | 1.6551 | 378 | 630 | 5.2 | 809 | 35.7 | 1.156 |
| 58: | 55.730 | 1.6481 | 55.734 | 1.6480 | 403 | 1037 | 8.5 | 1480 | 65.4 | 1.284 |
| 59: | 56.390 | 1.6304 | 56.390 | 1.6304 | 405 | 1129 | 9.3 | 970 | 42.9 | 0.773 |
| 60: | 57.440 | 1.6030 | 57.439 | 1.6030 | 444 | 90 | 0.7 | 21 | 0.9 | 0.210 |
| 61: | 58.840 | 1.5682 | 58.833 | 1.5684 | 328 | 234 | 1.9 | 208 | 9.2 | 0.800 |
| 62:: | 59.520 | 1.5519 | 59.527 | 1.5517 | 335 | 235 | 1.9 | 53 | 2.3 | 0.203 |
| 63: | 60.750 | 1.5234 | 60.752 | 1.5233 | 205 | 394 | 3.2 | 166 | 7.3 | 0.379 |
| 64: | 62.239 | 1.4904 | 62.248 | 1.4903 | 193 | 84 | 0.7 | 33 | 1.5 | 0.354 |
| 65: | 64.270 | 1.4482 | 64.284 | 1.4479 | 184 | 127 | 1.0 | 69 | 3.0 | 0.489 |
| 66: | 64.810 | 1.4374 | 64.828 | 1.4370 | 182 | 211 | 1.7 | 193 | 8.5 | 0.823 |
| 67: | 67.760 | 1.3818 | 67.766 | 1.3817 | 228 | 140 | 1.1 | 50 | 2.2 | 0.321 |
| 68: | 68.300 | 1.3722 | 68.301 | 1.3722 | 242 | 128 | 1.0 | 63 | 2.8 | 0.443 |

continued ...

TABLE B-3 (concluded)

| | Peak-Position | | Centroid-Position | | | Peak & Area are without Bkgrd* | | | | |
|---|---|---|---|---|---|---|---|---|---|---|
| # | 2Theta | d | 2Theta | d | Bkgrd | Peak | I% | Area | I% | FWHM |
| 69: | 69.650 | 1.3489 | 69.651 | 1.3489 | 261 | 404 | 3.3 | 247 | 10.9 | 0.550 |
| 70: | 72.530 | 1.3022 | 72.533 | 1.3022 | 222 | 87 | 0.7 | 35 | 1.5 | 0.362 |
| 71: | 74.840 | 1.2677 | 74.841 | 1.2676 | 350 | 97 | 0.8 | 36 | 1.6 | 0.334 |
| 72: | 75.749 | 1.2547 | 75.748 | 1.2547 | 388 | 216 | 1.8 | 49 | 2.2 | 0.204 |
| 73: | 76.620 | 1.2426 | 76.617 | 1.2426 | 377 | 217 | 1.8 | 329 | 14.5 | 1.365 |
| 74: | 77.590 | 1.2295 | 77.593 | 1.2294 | 382 | 223 | 1.8 | 461 | 20.4 | 1.861 |
| 75: | 78.090 | 1.2228 | 78.078 | 1.2230 | 411 | 161 | 1.3 | 50 | 2.2 | 0.280 |
| 76: | 79.009 | 1.2109 | 79.003 | 1.2110 | 352 | 115 | 0.9 | 61 | 2.7 | 0.477 |
| 77: | 80.319 | 1.1944 | 80.335 | 1.1942 | 238 | 118 | 1.0 | 49 | 2.2 | 0.374 |
| 78: | 85.950 | 1.1300 | 85.943 | 1.1301 | 244 | 87 | 0.7 | 45 | 2.0 | 0.466 |
| 79: | 87.240 | 1.1166 | 87.245 | 1.1165 | 240 | 298 | 2.4 | 433 | 19.1 | 1.308 |
| 80: | 87.520 | 1.1137 | 87.516 | 1.1138 | 237 | 222 | 1.8 | 191 | 8.4 | 0.774 |
| 81: | 88.310 | 1.1058 | 88.315 | 1.1057 | 249 | 228 | 1.9 | 158 | 7.0 | 0.624 |
| 82: | 88.560 | 1.1033 | 88.555 | 1.1034 | 248 | 223 | 1.8 | 171 | 7.6 | 0.690 |
| 83: | 91.270 | 1.0775 | 91.257 | 1.0776 | 208 | 102 | 0.8 | 35 | 1.5 | 0.309 |
| 84: | 94.090 | 1.0525 | 94.080 | 1.0526 | 286 | 201 | 1.6 | 67 | 3.0 | 0.300 |
| 85: | 94.390 | 1.0499 | 94.385 | 1.0500 | 259 | 109 | 0.9 | 50 | 2.2 | 0.413 |
| 86: | 94.740 | 1.0470 | 94.746 | 1.0469 | 231 | 116 | 1.0 | 326 | 14.4 | 2.529 |
| 87: | 95.750 | 1.0386 | 95.753 | 1.0386 | 256 | 137 | 1.1 | 139 | 6.1 | 0.913 |
| 88: | 112.840 | 0.9246 | 112.842 | 0.9246 | 370 | 242 | 2.0 | 67 | 3.0 | 0.249 |
| 89: | 113.280 | 0.9223 | 113.269 | 0.9223 | 397 | 114 | 0.9 | 24 | 1.1 | 0.189 |
| 90: | 115.350 | 0.9116 | 115.341 | 0.9116 | 373 | 181 | 1.5 | 117 | 5.2 | 0.582 |
| 91: | 115.759 | 0.9095 | 115.756 | 0.9095 | 390 | 52 | 0.4 | 7 | 0.3 | 0.121 |

* Intensity values are based on counts per second.

TABLE B-4

XRD DATA FOR $UO_2$ OXIDATION AT 150°C IN GAMMA RADIATION IN

(Ar + 60% Saturated Steam; Sample V, Experiment D)

| | Peak-Position | | Centroid-Position | | | Peak & Area are without Bkgrd* | | | | |
|---|---|---|---|---|---|---|---|---|---|---|
| # | 2Theta | d | 2Theta | d | Bkgrd | Peak | I% | Area | I% | FWHM |
| 1: | 28.270 | 3.1543 | 28.263 | 3.1550 | 78 | 41947 | 100.0 | 12329 | 100.0 | 0.265 |
| 2: | 32.760 | 2.7315 | 32.761 | 2.7315 | 53 | 18163 | 43.3 | 4400 | 35.7 | 0.218 |
| 3: | 46.970 | 1.9329 | 46.977 | 1.9327 | 48 | 19586 | 46.7 | 6100 | 49.5 | 0.280 |
| 4: | 55.720 | 1.6484 | 55.724 | 1.6483 | 84 | 18495 | 44.1 | 5686 | 46.1 | 0.277 |
| 5: | 55.840 | 1.6451 | 55.840 | 1.6451 | 86 | 9733 | 23.2 | 2559 | 20.8 | 0.237 |
| 6: | 58.420 | 1.5784 | 58.424 | 1.5783 | 75 | 4117 | 9.8 | 1336 | 10.8 | 0.292 |
| 7: | 58.560 | 1.5750 | 58.560 | 1.5750 | 73 | 2118 | 5.0 | 523 | 4.2 | 0.222 |
| 8: | 68.600 | 1.3669 | 68.600 | 1.3669 | 26 | 3278 | 7.8 | 863 | 7.0 | 0.237 |
| 9: | 68.790 | 1.3636 | 68.787 | 1.3637 | 27 | 1635 | 3.9 | 393 | 3.2 | 0.216 |
| 10: | 75.760 | 1.2545 | 75.759 | 1.2545 | 105 | 6705 | 16.0 | 2023 | 16.4 | 0.272 |
| 11: | 75.970 | 1.2516 | 75.968 | 1.2516 | 112 | 3191 | 7.6 | 772 | 6.3 | 0.218 |
| 12: | 78.100 | 1.2227 | 78.097 | 1.2227 | 95 | 5218 | 12.4 | 1535 | 12.5 | 0.265 |
| 13: | 78.320 | 1.2198 | 78.317 | 1.2199 | 91 | 2522 | 6.0 | 584 | 4.7 | 0.208 |
| 14: | 87.270 | 1.1163 | 87.266 | 1.1163 | 48 | 5203 | 12.4 | 1818 | 14.7 | 0.314 |
| 15: | 87.530 | 1.1136 | 87.523 | 1.1137 | 49 | 2475 | 5.9 | 744 | 6.0 | 0.271 |
| 16: | 94.080 | 1.0526 | 94.081 | 1.0526 | 51 | 5172 | 12.3 | 1718 | 13.9 | 0.299 |
| 17: | 94.390 | 1.0499 | 94.380 | 1.0500 | 50 | 2445 | 5.8 | 725 | 5.9 | 0.267 |
| 18 : | 104.960 | 0.9712 | 104.974 | 0.9711 | 41 | 128 | 0.3 | 161 | 1.3 | 1.132 |
| 19: | 105.630 | 0.9669 | 105.628 | 0.9669 | 43 | 1773 | 4.2 | 671 | 5.4 | 0.341 |
| 20: | 106.010 | 0.9645 | 106.003 | 0.9645 | 49 | 778 | 1.9 | 256 | 2.1 | 0.296 |
| 21: | 112.850 | 0.9245 | 112.850 | 0.9246 | 155 | 5677 | 13.5 | 2082 | 16.9 | 0.330 |
| 22: | 113.280 | 0.9223 | 113.275 | 0.9223 | 175 | 2496 | 6.0 | 768 | 6.2 | 0.277 |
| 23: | 114.350 | 0.9167 | 114.359 | 0.9166 | 193 | 47 | 0.1 | 5 | 0.0 | 0.096 |
| 24: | 115.340 | 0.9116 | 115.338 | 0.9116 | 146 | 3051 | 7.3 | 1080 | 8.8 | 0.319 |
| 25: | 115.790 | 0.9094 | 115.785 | 0.9094 | 132 | 1335 | 3.2 | 402 | 3.3 | 0.271 |

* Intensity values are based on counts per second.

Cat. No./N° de cat.: CC2-11351E
ISBN 0-660-16193-1
ISSN 0067-0367

To identify individual documents in the series, we have assigned an AECL-number to each. Please refer to the AECL-number when requesting additional copies of this document from:

Scientific Document Distribution Office (SDDO)
AECL
Chalk River, Ontario
Canada K0J 1J0

Fax: (613) 584-1745 Tel.: (613) 584-3311
ext. 4623

Price: B

Pour identifier les rapports individuels faisant partie de cette série, nous avons affecté un numéro AECL-à chacun d'eux. Veuillez indiquer le numéro AECL-lorsque vous demandez d'autres exemplaires de ce rapport au

Service de distribution des documents officiels (SDDO)
EACL
Chalk River (Ontario)
Canada K0J 1J0

Fax: (613) 584-1745 Tél.: (613) 584-3311
poste 4623

Prix: B